Supporting Information

Development of Site-specific Mg^{2+}-RNA Force Field Parameters: A Dream or Reality? Guidelines from Combined Molecular Dynamics and Quantum Mechanics Simulations

*Lorenzo Casalino,[1] Giulia Palermo,[2†] Nodira Abdurakhmonova,[1,3] Ursula Rothlisberger,[2] Alessandra Magistrato[4]**

1. International School for Advanced Studies (SISSA), Trieste, Italy

2. Laboratory of Computational Chemistry and Biochemistry, Institute of Chemical Sciences and Engineering, École Polytechnique Fédérale de Lausanne, CH-1015 Lausanne, Switzerland

3. Università degli Studi di Trieste, Trieste, Italy.

4. CNR-IOM-Democritos national simulation center c/o SISSA, via Bonomea 265, Trieste, Italy

† present address: University of California at San Diego 9500 Gilman Dr., M/C 0365. La Jolla, CA 92093-0365.

Table of contents

Corresponding author: Dr. Alessandra Magistrato (alessandra.magistrato@sissa.it)

1. Supplementary Material

1.1 Computational Details

Among the non-bonded fixed point charge, we selected the parametrization due to Åqvist,[1] which has been originally developed to reproduce the solvation free energy and radial distribution function *(g(r))* of aqueous Mg^{2+} ions, the recent model developed by Allnér et al.,[2] in which Mg^{2+} parameters have been tuned to reproduce the experimental first shell water/phosphate exchange rate and the parameters developed by Li et al.,[3] which are specific for Particle Mesh Ewald-based simulations. In particular, for the latter we chose the parameter set better accounting for Mg^{2+} coordination number and hydration free energy (i.e., the CN set for TIP3P water).[3] Among the cationic dummy atom (CDA) models, we have considered the one from Oelschlaeger et al.[4] and Saxena et al.[5] The former assigns a charge -1 to the central atom, while the surrounding dummy atoms, disposed as octahedron, have a fractional positive charge accounting for +3. The Saxena model distributes the +2 charge entirely among the dummies, which are given only a repulsive "A coefficient" for the vdW potential. FF parameters for fixed point charge and CDA models are reported in Table S1. In the Amber FF, vdW interactions are calculated according to the simplified Lennard-Jones potential $V_{L-J} = \frac{A_{ij}}{r^{12}} - \frac{B_{ij}}{r^6}$, where $A_{ij} = \varepsilon_{ij}\left(R_{\min,ij}\right)^{12}$ is the repulsive term and $B_{ij} = 2\varepsilon_{ij}\left(R_{\min,ij}\right)^{6}$ is the attractive term. ε_{ij} and $R_{min,ij}$ correspond to the energy minimum (i.e., the depth of the potential well) and the internuclear separation between species i and j at the energy minimum, respectively. ε_{ij} and $R_{min,ij}$ are calculated by means of Lorentz-Berthelot mixing rules in which $\varepsilon_{ij} = \sqrt{\varepsilon_i \varepsilon_j}$ and $R_{\min,ij} = \left(R_{min,ii} + R_{min,jj}\right)/2$. The self-interaction values for $A_{Mg\text{-}Mg}$ and $B_{Mg\text{-}Mg}$ for each parametrization, as calculated in the Amber FF, are reported in the Table S1 ($A_{d\text{-}d}$ and $B_{d\text{-}d}$ for dummy atom species), together with the assigned point charge for Mg^{2+} ion/central atom (i.e., q_{Mg}) and, where necessary, for the dummy atoms (i.e., q_d).

1.2 Radial distribution function

Analysis of $g_{Mg\text{-}X}(r)$ (Figure S5 and Table S2) displays a contraction of the Mg^{2+}-X bonds for the Åqvist parametrization in which the first peak is split in two: one corresponding to the Mg^{2+}-O_{ph} coordination distance, and the other to the remaining

coordinating ligands lying at slightly higher *r* value. The Saxena model reveals a similar pattern of the *g(r)*, shifted toward larger values of the radial distances. In the Allnér and Li models the *g(r)* profile exhibits a single well defined first peak, lying at slightly larger values than the one obtained with the Åqvist FF. Also for these parametrizations, the distances between Mg^{2+} and its ligands are underestimated in all cases, while the Mg^{2+}-N_b distance is again overestimated in Allnér. For the Oelschlaeger parametrization, a different *g(r)* is observed, showing a broad first peak shifted toward larger values of *r* with respect to all other models. This corresponds to unrealistically large distances between Mg^{2+} and its ligands.

1.3 The Catalytic Mg^{2+}-aided Active Site.

Group II intron ribozyme (G*II*-I) presents a peculiar catalytic site which enables the intron self-splicing reaction.[6] The importance of this site is associated to a two-Mg^{2+}-aided mechanism that is also exploited by the spliceosome and is therefore critical in regulating gene expression in humans. The peculiar *GII*-I active site, characterized by the presence of two Mg^{2+} at a ~4 Å distance[6] (Figure S21), is not reported among the CPs classified by Zheng et al.[7] because of its low statistical abundance, which is most likely associated to its very specific biological function.[7-9]

Our molecular simulations reveal that only the Åqvist and the Saxena FFs are capable of reproducing a catalytically competent conformation of the two-metal-aided active site (Figure S22), consistent with the X-ray structure. Surprisingly, by employing the Allnér parameters, the active site distorts after a few nanoseconds of MD (i.e., ~10 ns, Figure S23). The Allnér model has been tuned to reproduce the kinetics of Mg^{2+}-water/phosphate exchange reactions and presents a lower free energy barrier for water exchange than the Åqvist model.[2] This may determine the structural instability of the catalytic site, which is largely solvent exposed. Additionally, the vicinity of the two catalytic Mg^{2+} ions (~4 Å) leads to a strong electrostatic repulsion, which may favor Mg^{2+}-water/phosphate exchange and the structural distortion of the active site. A CDA model as the one due to Saxena succeeds in limiting these instabilities by spreading the 2+ charge among the dummy atoms in the direction of the coordinating donor atoms. At increased Mg^{2+} ions concentration (i.e., 25 mM) one of the metal ions (i.e., Mg^{2+}-A)

looses its original coordination geometry even with the Åqvist parameters, although no additional ions locate in the vicinity of the binding site (Figure S22), while the geometry is retained with the Saxena model. Overall, these data indicate that the choice of the classical parameters for Mg^{2+} ions in metal-dependent active sites can be influenced by the structural characteristics of the site itself and, importantly, by the experimental working conditions relative to Mg^{2+} concentration.

2. Supplementary Figures

2.1 Group II Intron Ribozyme

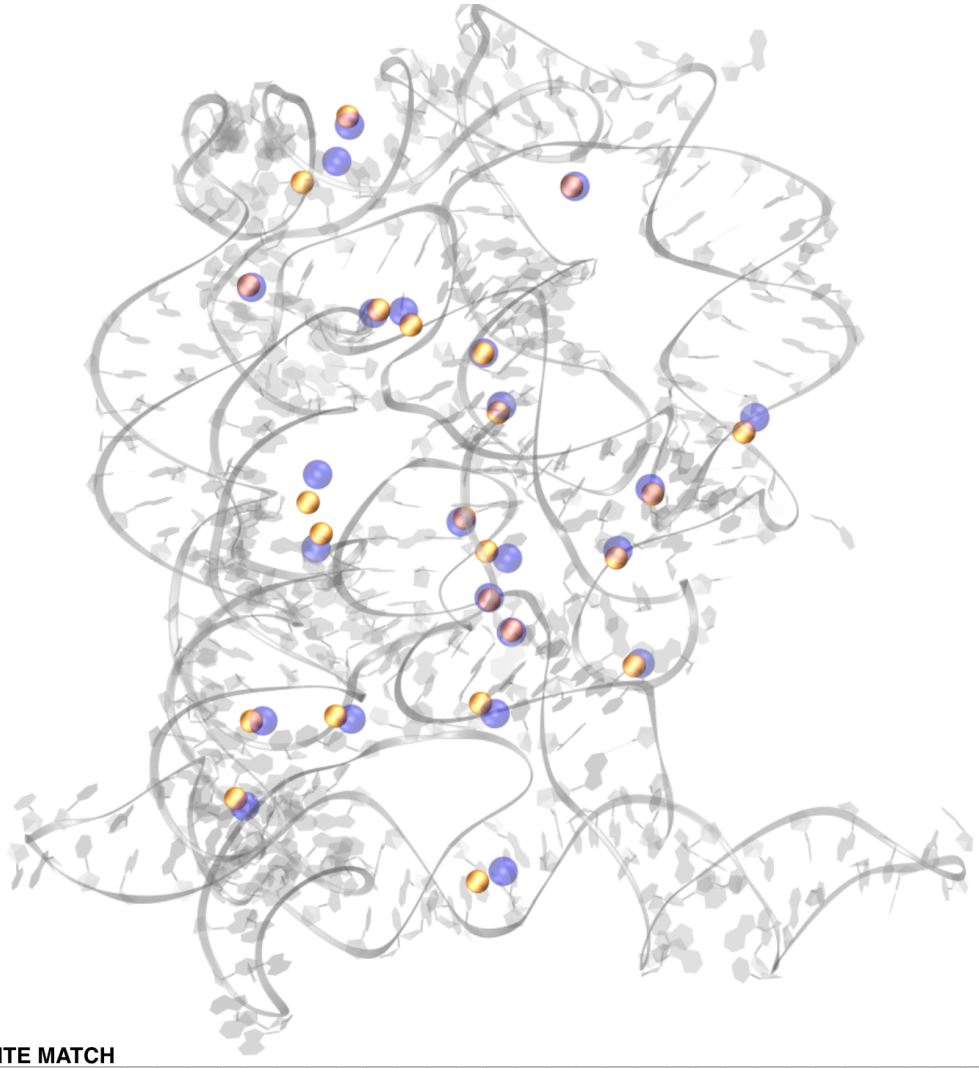

SITE MATCH

#	1	2	3	4	5	6	7	8	9	10	11	12	13	14	15	16	17	18	19	20	21	22	23	24	25	26	27	28	29	30
PDB 4FAQ (Ca^{2+})	401	402	403	404	405	406	407	408	409	410	411	412	413	414	415	416	417	418	419	420	421	422	423	-						
PDB 4FAR (Mg^{2+})	431	401	405	407	408	409	410	411	412	413	414	416	425	419	420	421	422	423	406	427	428	429	417	-	-	-	-	-	-	-

Figure S1. Superposition between the 4FAQ and 4FAR X-ray structures of group II intron ribozyme (G*II*-I),[10] which have been crystallized in the presence of Ca^{2+} and Mg^{2+} ions, respectively. Ca^{2+} (4FAQ) and Mg^{2+} (4FAR) ions are shown as blue and orange van der Waals spheres. The overall architecture of G*II*-I is represented as gray ribbons. In the table, the ions (i.e., Ca^{2+} and Mg^{2+}) which have a site match among the two structures are reported with the numbering scheme as in the two X-ray structures (blue and orange lines). The sign "-" refers to the ions which do not have a match.

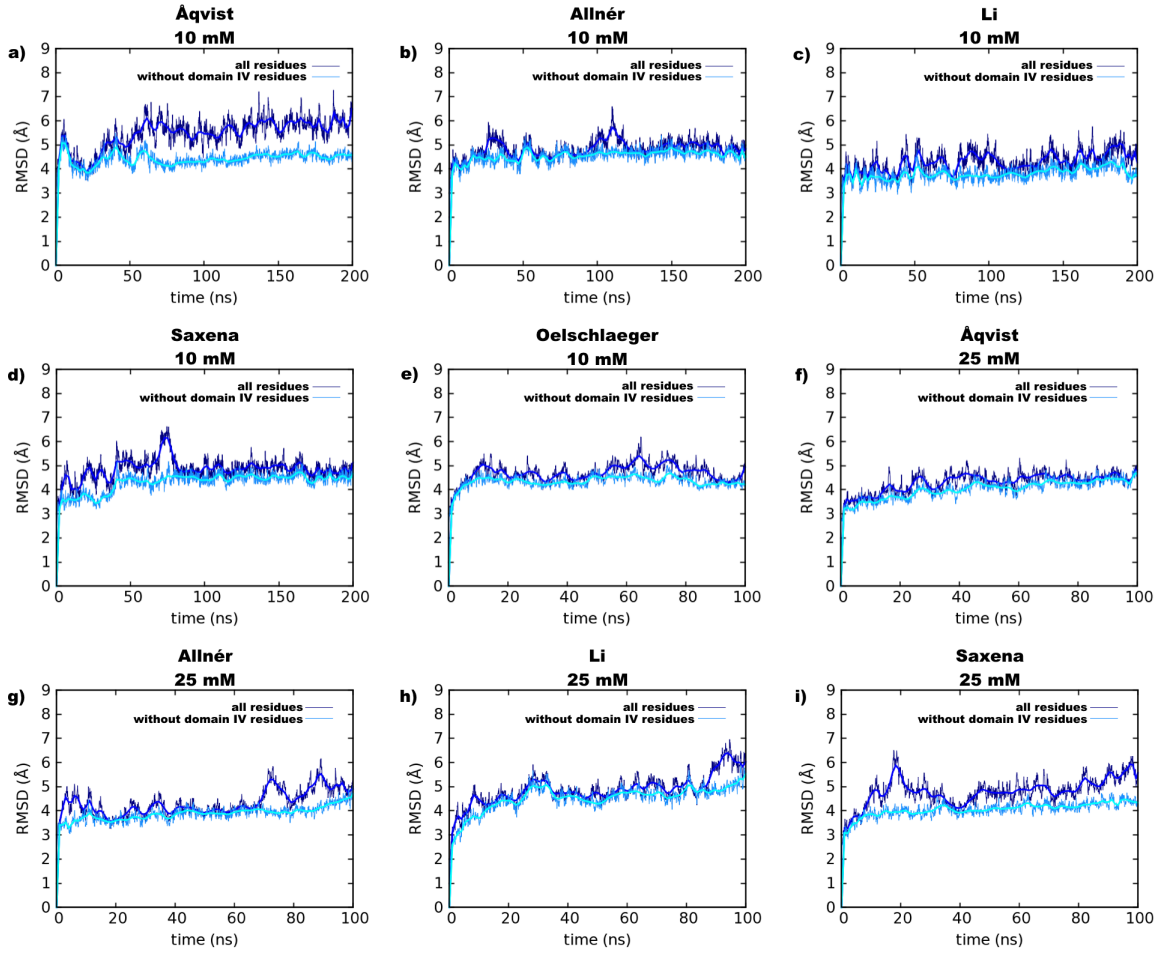

Figure S2. RMSD (Å) vs simulation time (ns) of the catalytically competent form of group II intron ribozyme with empirical Mg^{2+} force field parameters according to the Åqvist, Allnér, Li, Saxena and Oelschlaeger models in (a), (b), (c), (d) and (e), respectively, at [Mg^{2+}] = 10 mM, and to the Åqvist, Allnér, Li and Saxena models in (f), (g), (h) and (i), respectively, at [Mg^{2+}] = 25 mM. The RMSD without residues of the domain IV is reported with the light blue line. This part of the ribozyme is highly solvent exposed and is responsible in some case of the oscillatory behavior of the RMSD.

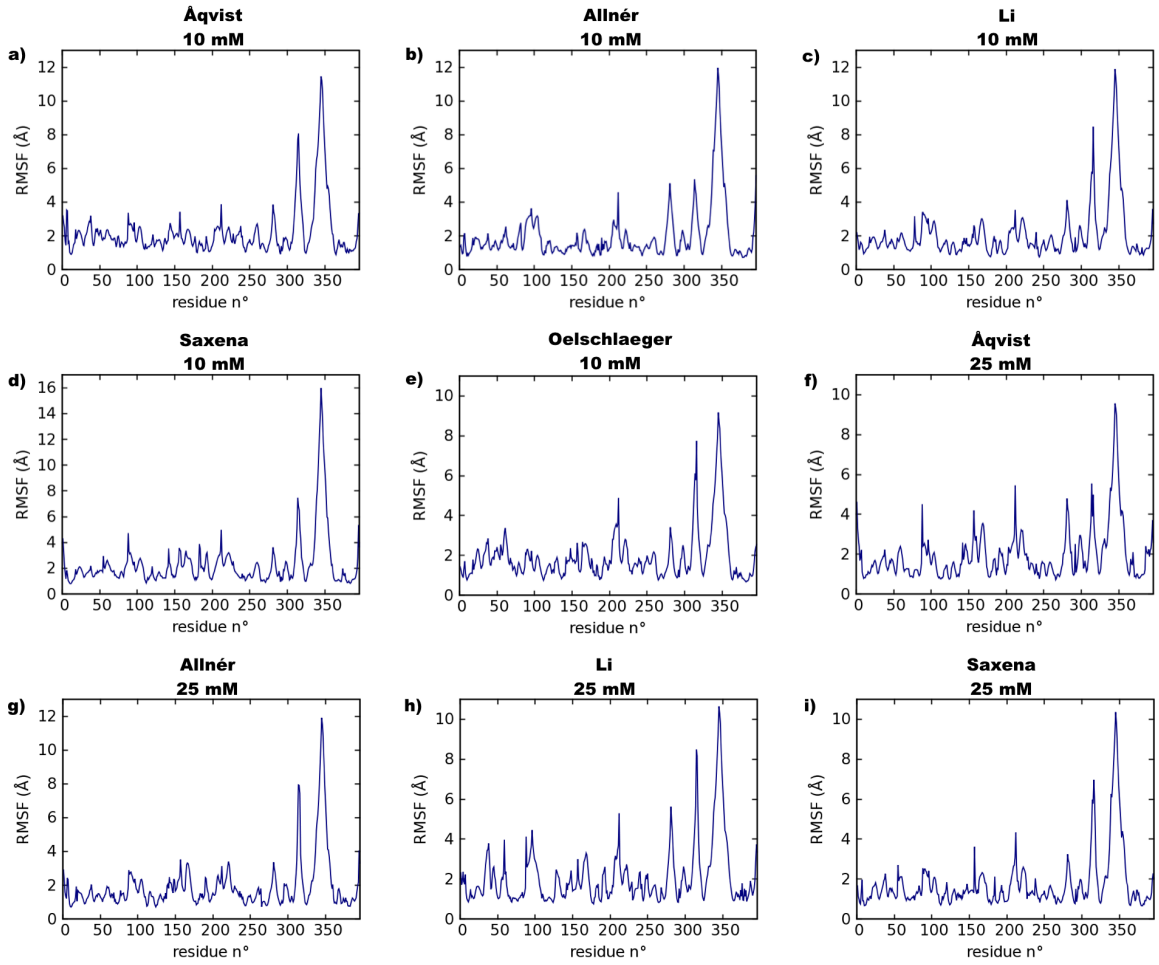

Figure S3. RMSF (Å) vs residue number of the catalytically competent form of group II intron ribozyme with empirical Mg^{2+} force field parameters according to the Åqvist, Allnér, Li, Saxena and Oelschlaeger models in (a), (b), (c), (d) and (e), respectively, at $[Mg^{2+}]$ = 10 mM, and to the Åqvist, Allnér, Li and Saxena models in (f), (g), (h) and (i), respectively, at $[Mg^{2+}]$ = 25 mM.

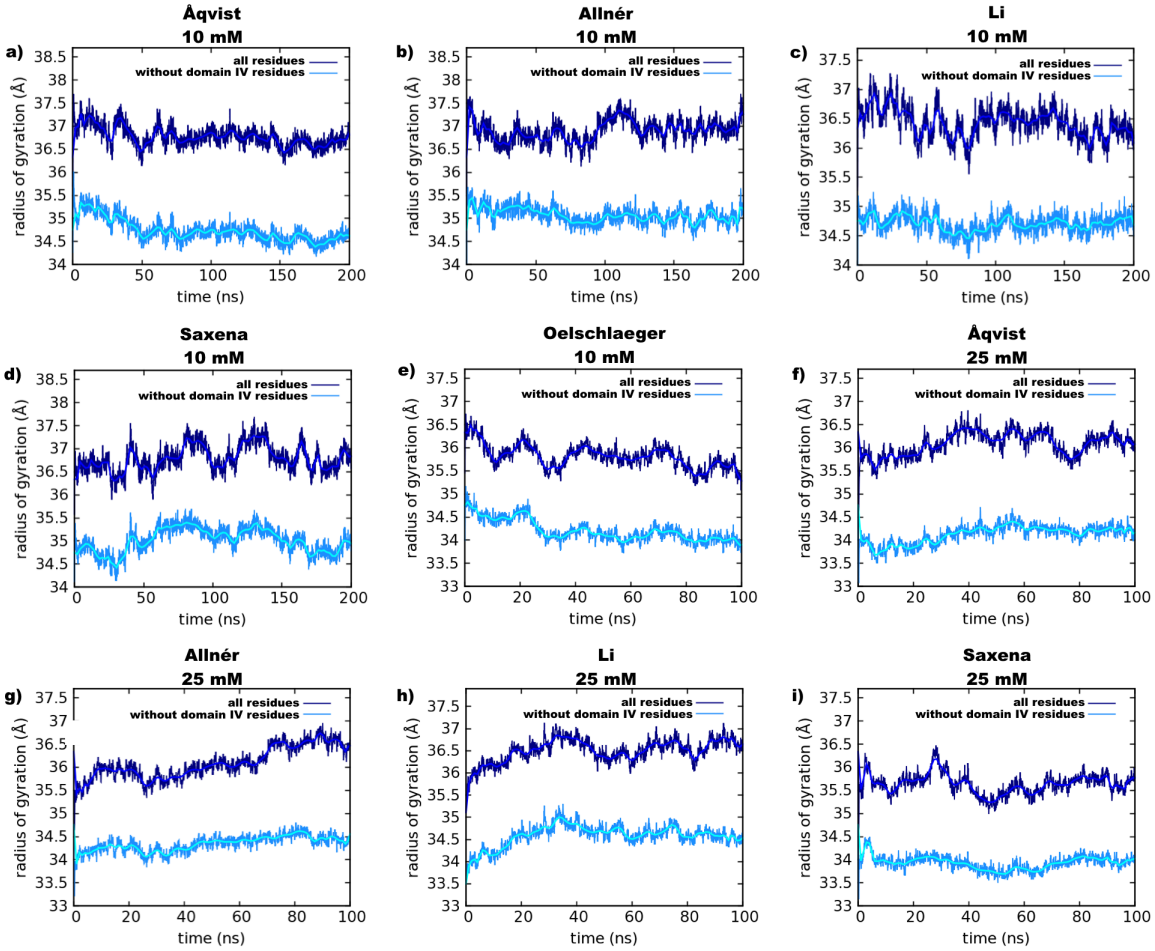

Figure S4. Radius of gyration (R_g) (Å) vs simulation time (ns) of the catalytically competent form of group II intron ribozyme with empirical Mg^{2+} force field parameters according to the Åqvist, Allnér, Li, Saxena and Oelschlaeger models in (a), (b), (c), (d) and (e), respectively, at [Mg^{2+}] = 10 mM, and to the Åqvist, Allnér, Li and Saxena models in (f), (g), (h) and (i), respectively, at [Mg^{2+}] = 25 mM. The R_g without residues of the domain IV is reported with the light blue line. This part of the ribozyme is highly solvent exposed and is responsible in some case of the oscillatory behavior of the R_g.

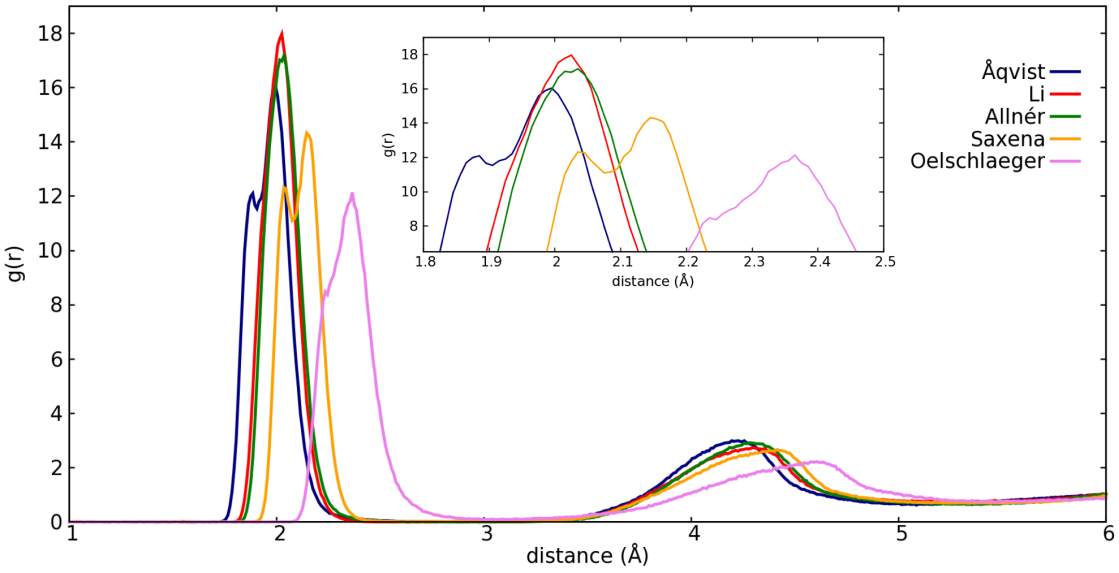

Figure S5. Radial distribution function (*g(r)*) for Mg^{2+} ions within 6 Å of their coordination sphere (including the O_{ph}, N_b, O_b, O_s and O_w ligands), calculated over MD simulations of G*II*-I ribozyme, performed with the Åqvist (blue), Allnér (green), Li (red), Saxena (orange) and Oelschlaeger (magenta) parameters at [Mg^{2+}] = 10 mM.

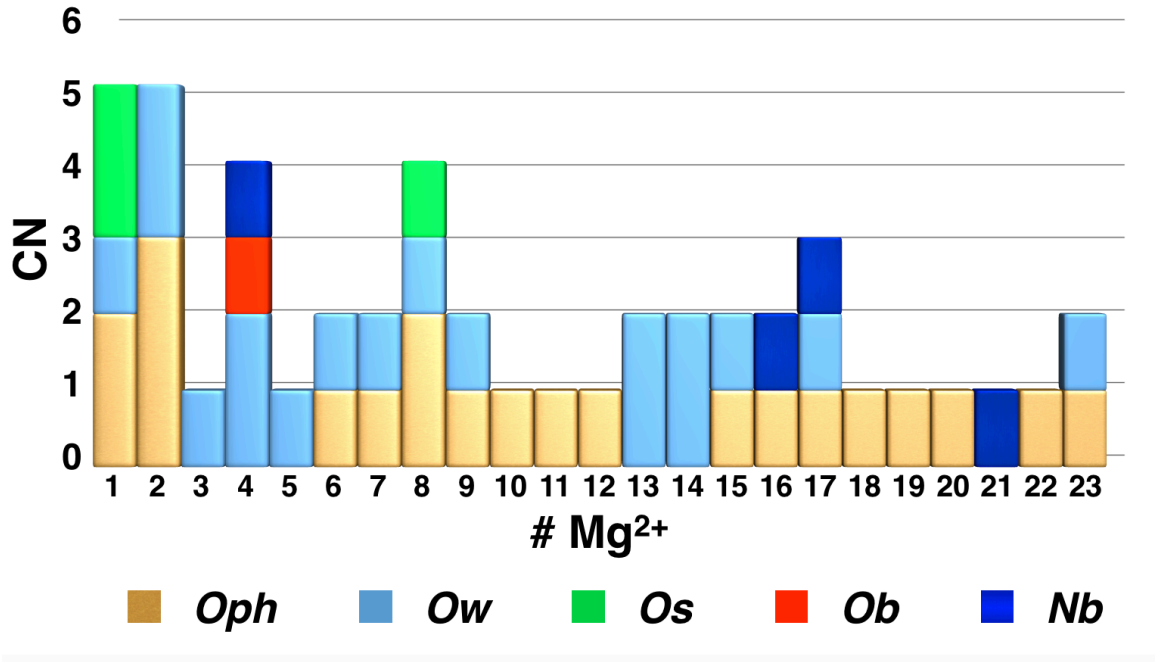

Figure S6. Histograms showing the ligand composition of the coordination sphere of each Mg^{2+} site in G*II*-I as found in the 4FAR[10] X-ray structure. In the *x-axis*, binding sites are renumbered according to the numbering of our simulated structure (4FAQ). Namely only the Mg^{2+} sites of 4FAR matching with Ca^{2+} sites of 4FAQ structure are reported, with internal numeration from #1 to #23 according to Figure S1. The *y-axis* reports the coordination number (*CN*) for each Mg^{2+} binding site. The limited resolution of the X-ray structure (i.e., 2.8 Å) impedes the complete dissection of the coordination sites.

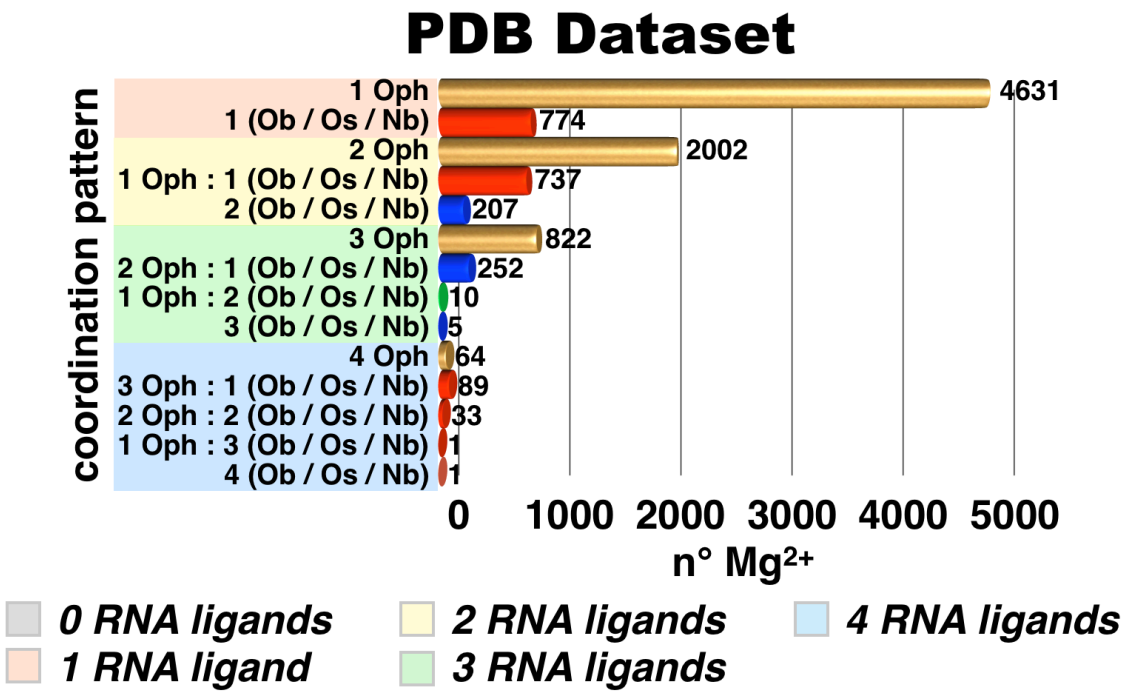

Figure S7. Histogram showing the population of Mg^{2+}-RNA coordination patterns extracted from Zheng et al.[7] for the whole PDB dataset (*y-axis*). The number of RNA ligands (from 0 to 4) is highlighted with different colors, as specified in the bottom legend. The *x-axis* reports the number of Mg^{2+} ions (i.e., population) having a specific coordination pattern. Bars of different colors are used to identify coordination patterns characterized by the presence of different ligand types: only O_{ph} (gold) or at least one O_b (red, if in majority with respect to sites containing at least one O_s or N_b), O_s (green, if in majority) or N_b (blue, if in majority) ligand.

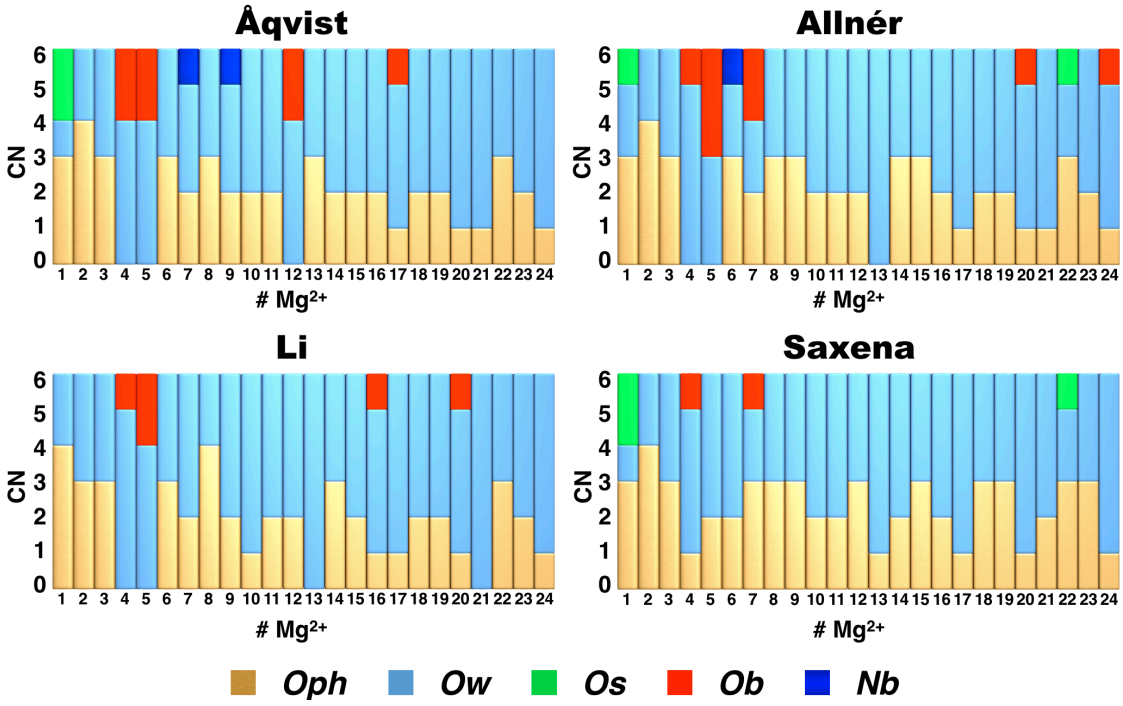

Figure S8. Histograms showing the composition of the first coordination sphere of each of the 24 Mg^{2+} sites in G*II*-I as determined from MD performed with the Åqvist, Allnér, Li and Saxena parametrizations at [Mg^{2+}] = 10 mM. The *x-axis* reports the 24 Mg^{2+} sites in G*II*-I, including sites 1 and 2, which are constitutive of the catalytic binuclear site. The *y-axis* reports the *CN* for the Mg^{2+} coordination sphere. Donor atom types are identified with different colors as specified in the bottom legend.

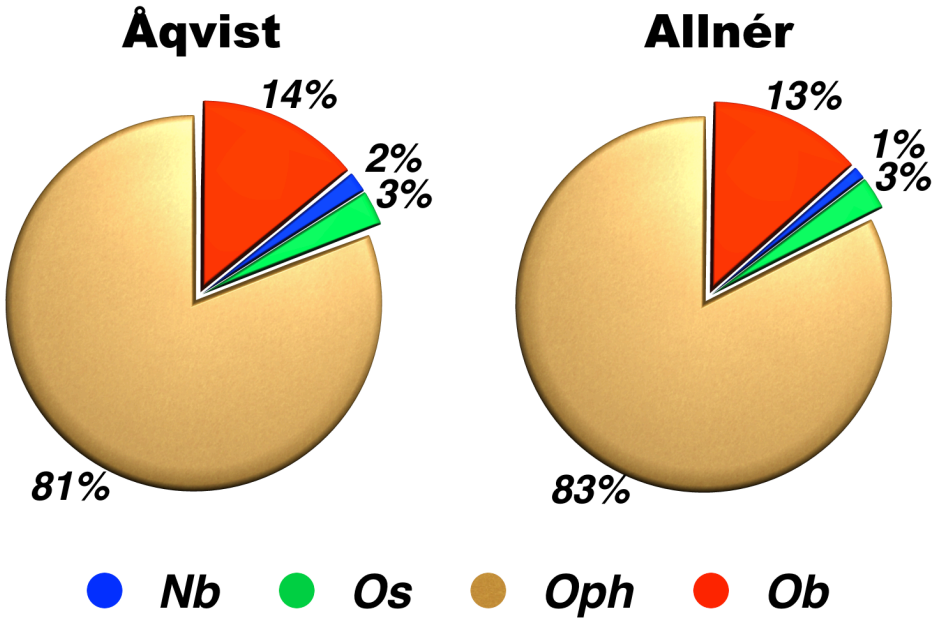

Figure S9. Statistical distribution of the Mg^{2+}–X ligands (where X = O_{ph}, N_b, O_b and O_s) in the Mg^{2+} *inner-sphere* (expressed as percentages), obtained from the combination of three different replicas of G*II*-I, performed with the Åqvist and Allnér parametrizations at [Mg^{2+}] = 10 mM. Donor atom types are identified with different colors as specified in the bottom legend.

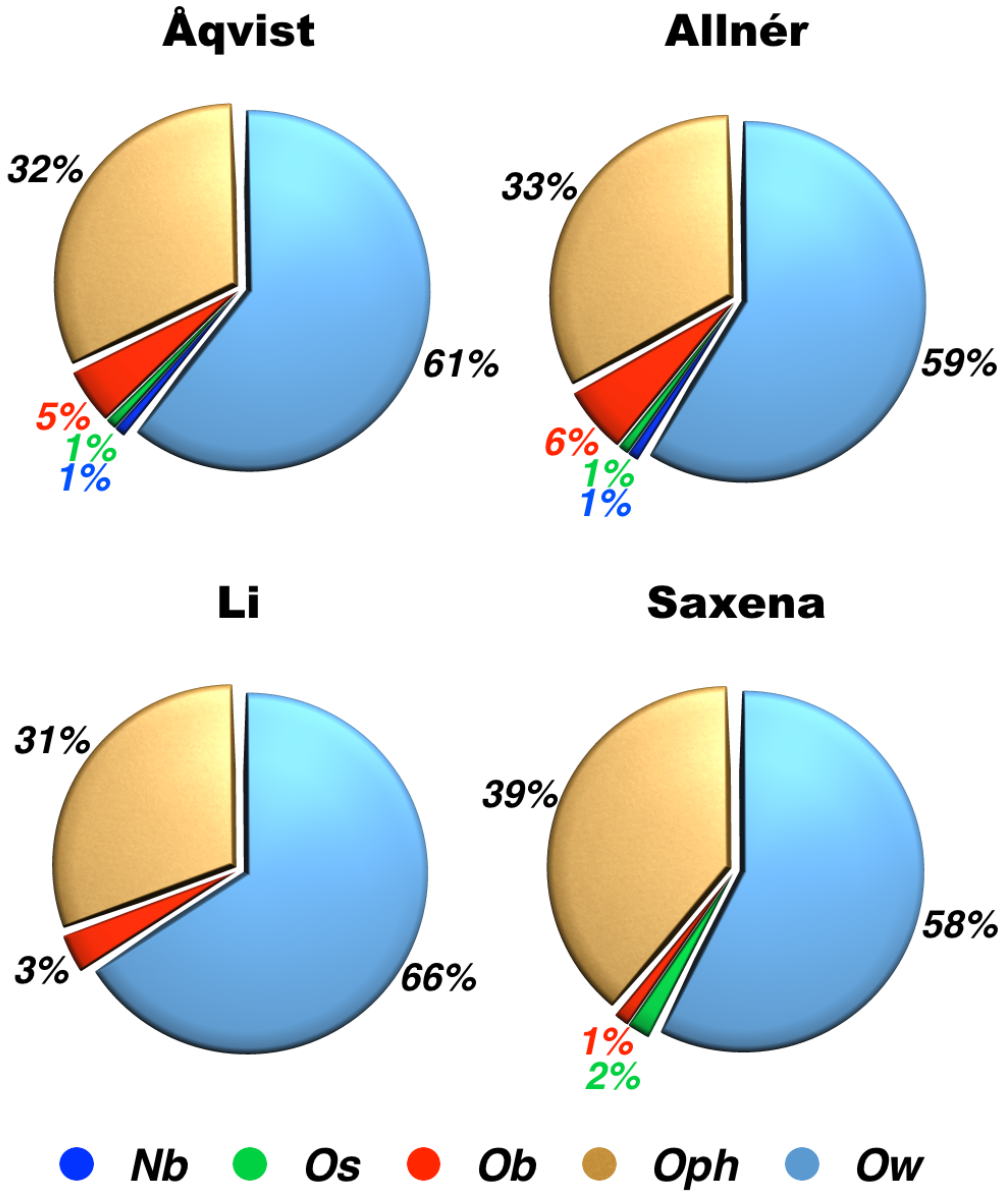

Figure S10. Statistical distribution of the Mg^{2+}–X ligands (where X = O_{ph}, N_b, O_b, O_s and O_w) in the Mg^{2+} *inner-sphere* (expressed as percentages) as calculated from MD simulations of G*II*-I performed with the Åqvist, Allnér, Li and Saxena parametrizations at [Mg^{2+}] = 10 mM. Donor atom types are identified with different colors as specified in the bottom legend. Remarkably, the Mg^{2+}–X statistical distribution is almost identical in the simulations performed with the Åqvist and Allnér parametrizations, while the occurrence of water ligands increases in Li and decreases in the Saxena model.

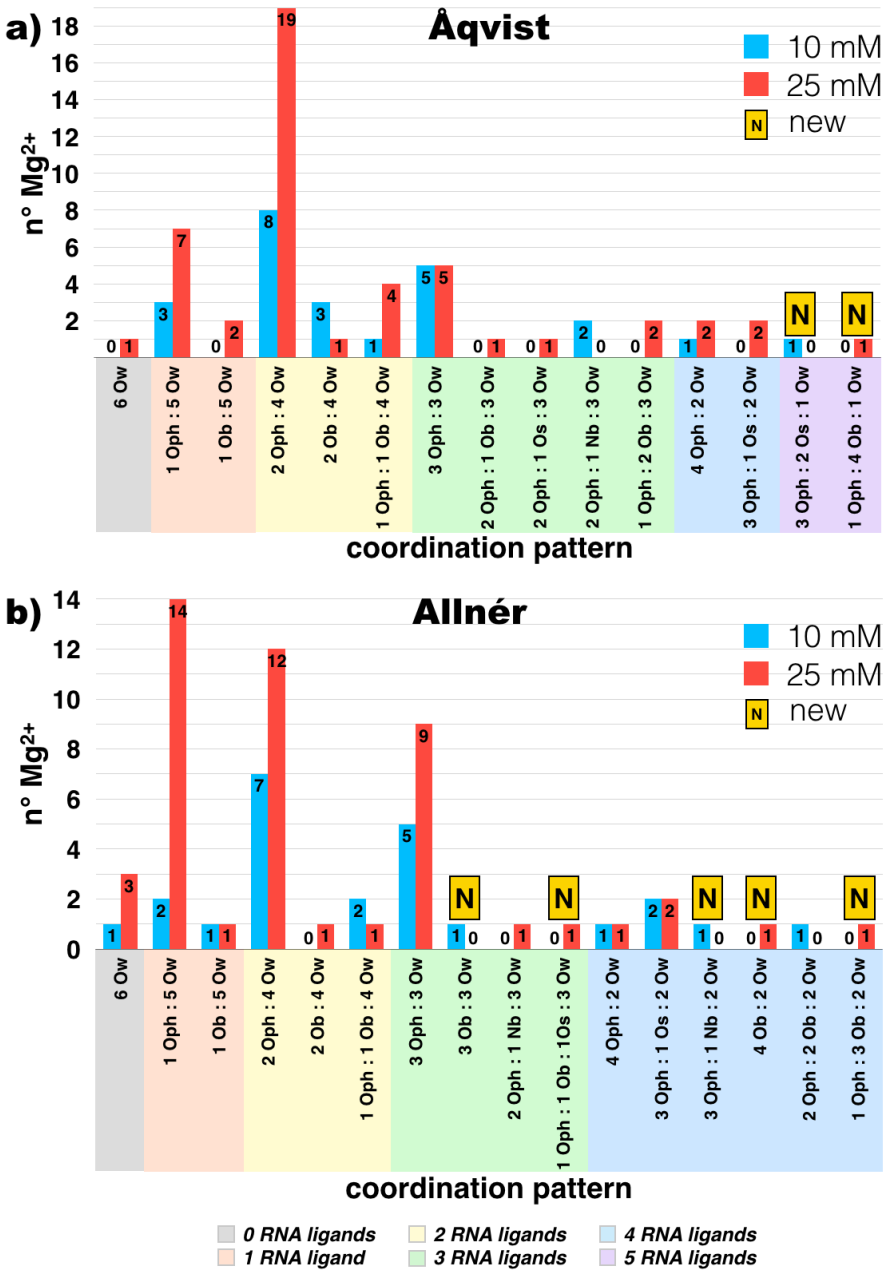

Figure S11. Histograms determining the population of the Mg^{2+}–RNA CPs, observed during MD simulations of G*II*-I, performed with the Åqvist (a) and Allnér (b) models at [Mg^{2+}] = 10 mM (blue bars) and 25 mM (red bars). The *x-axis* reports the Mg^{2+} CPs identified from MD simulations. The number of RNA ligands (from 0 to 5) is highlighted with different colors as shown in the bottom legend. The *y-axis* reports the number of Mg^{2+} ions (i.e., population) having a specific CP. The label N refers to binding sites not observed in the PDB dataset.

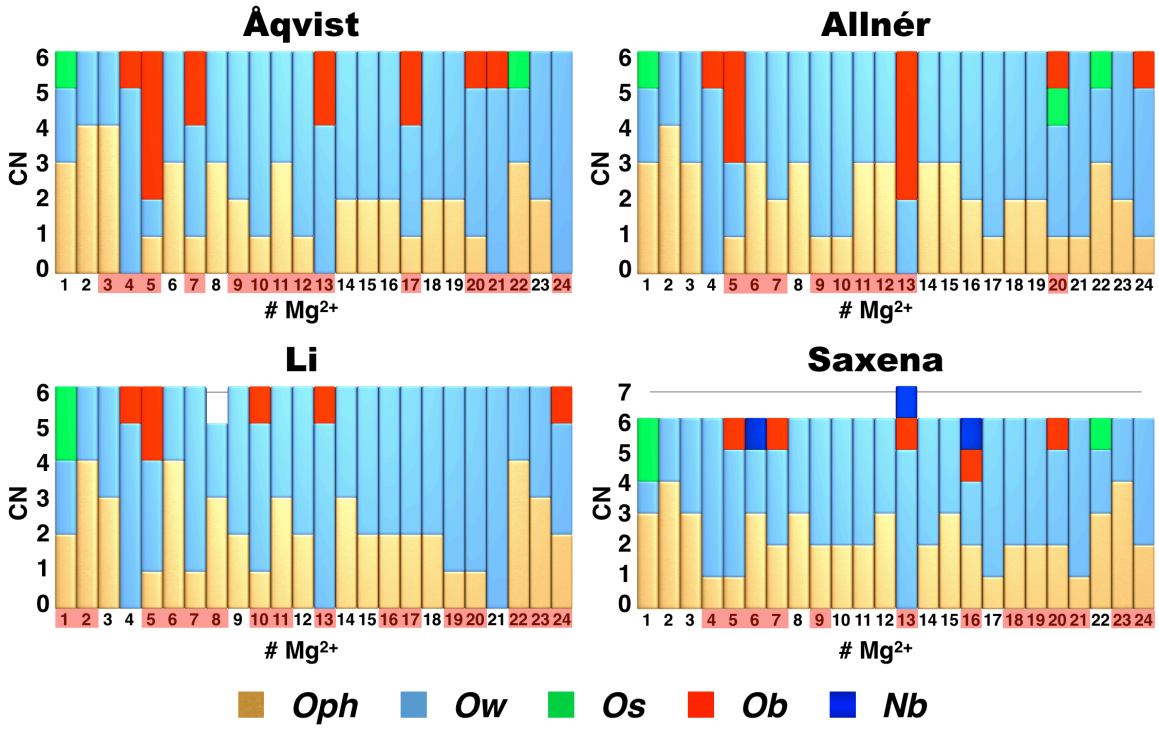

Figure S12. Histograms showing the composition of the coordination sphere of each of the first 24 out of 48 Mg^{2+} sites in G*II*-I as determined from MD performed with the Åqvist, Allnér, Li and Saxena parametrizations at [Mg^{2+}] = 25 mM. The *x-axis* reports the 24 Mg^{2+} sites in G*II*-I, including sites 1 and 2, which are constitutive of the catalytic site. The sites changing their ligand composition with respect to the simulation at [Mg^{2+}] = 10 mM are highlighted in red. Donor atom types are identified with different colors as specified in the bottom legend. The *y-axis* reports the *CN* for the Mg^{2+} coordination sphere. 63% of the sites exhibits the same composition at the two Mg^{2+} concentrations with the Allnér model, followed by Saxena (46 %), Åqvist (42%) and Li (33%).

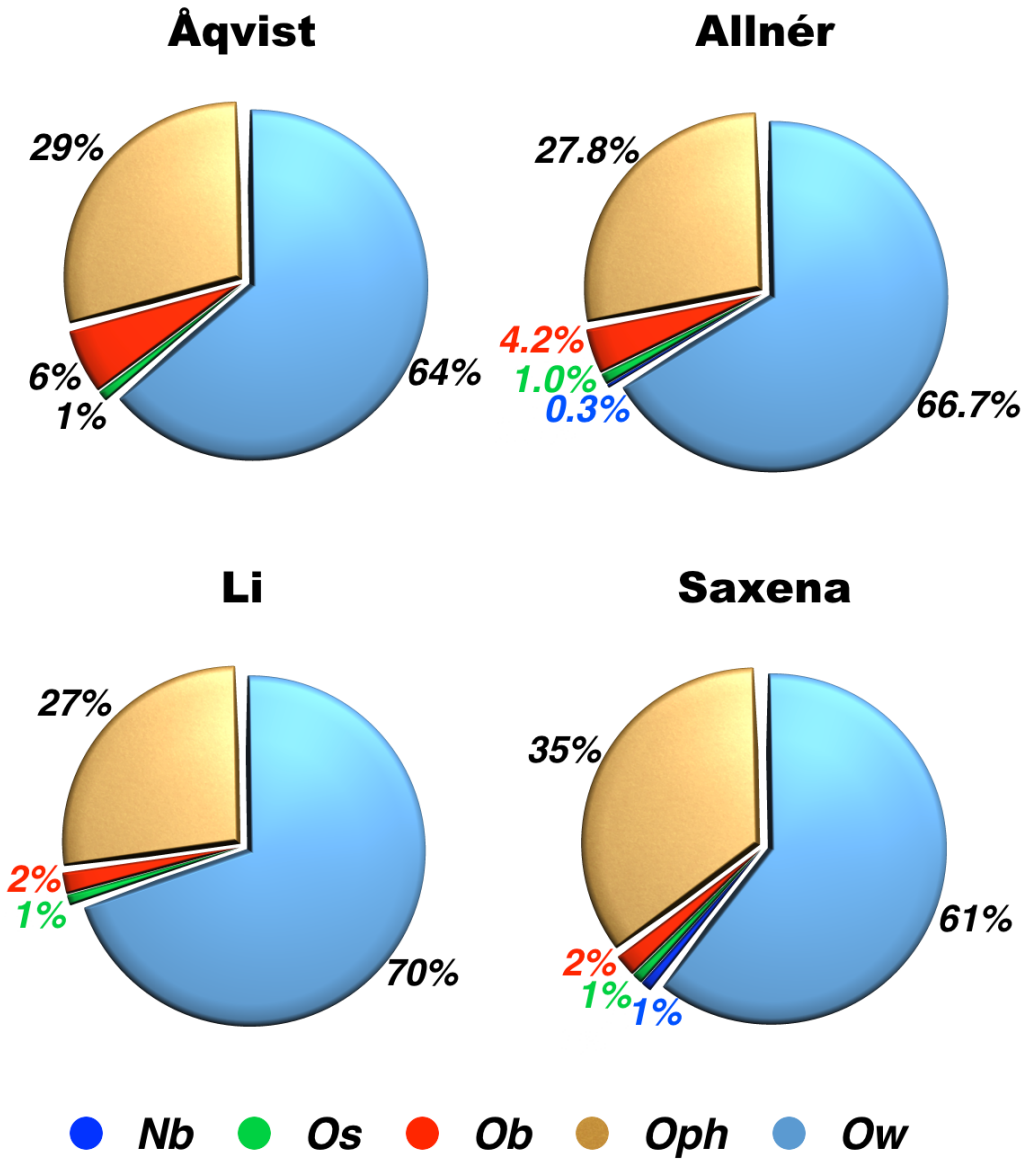

Figure S13. Statistical distribution of the Mg^{2+}–X ligands (where X = O_{ph}, N_b, O_b, O_s and O_w) in the Mg^{2+} *inner-sphere* (expressed as percentages) as calculated from MD simulations of G*II*-I performed with the Åqvist, Allnér, Li and Saxena parametrizations at [Mg^{2+}] = 25 mM. Donor atom types are identified with different colors as specified in the bottom legend.

2.2 Hepatitis Delta Virus Ribozyme

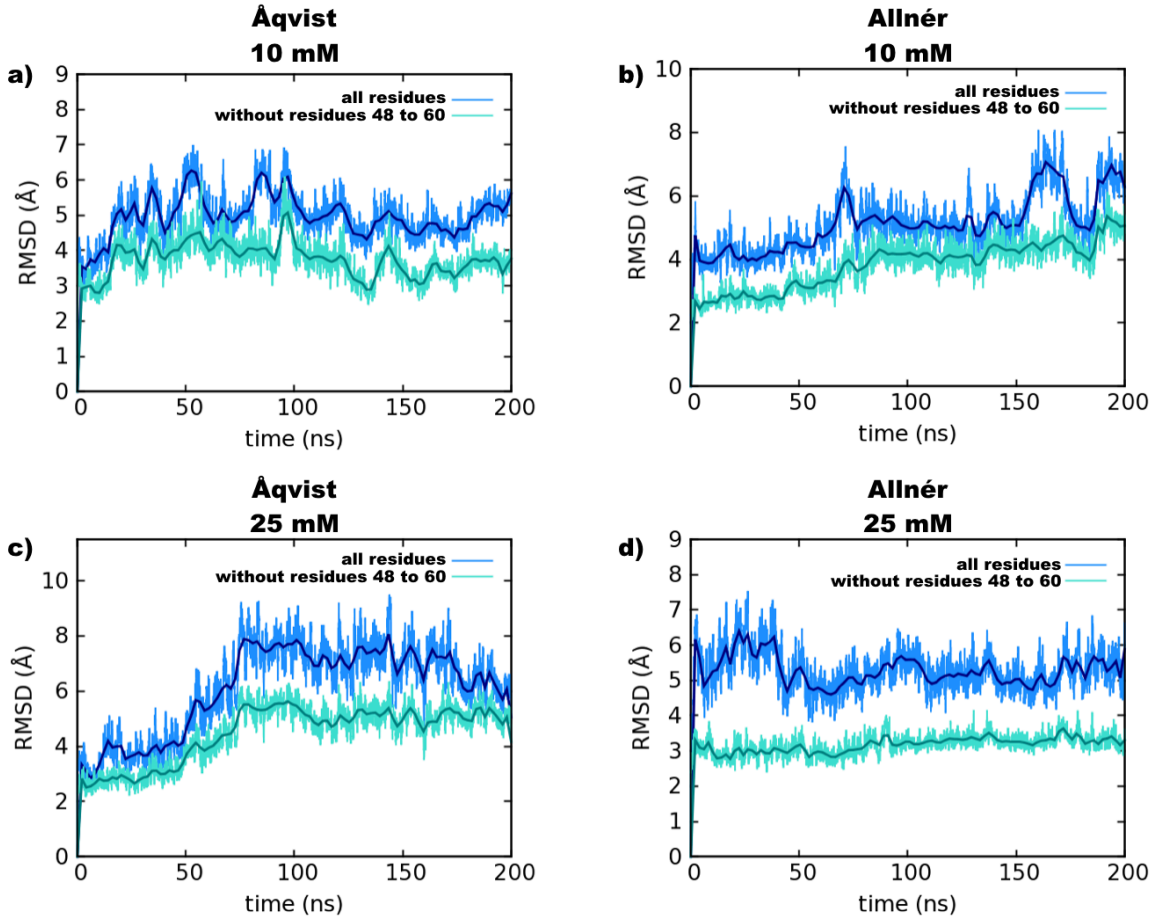

Figure S14. RMSD (Å) vs simulation time (ns) of the hepatitis delta virus (HDV) ribozyme with empirical Mg^{2+} force field parameters according to the Åqvist and Allnér models in (a) and (b), respectively, at $[Mg^{2+}]$ =10 mM and to the Åqvist and Allnér in (c) and (d), respectively, at $[Mg^{2+}]$ = 25 mM. The RMSD without residues 48 to 60 is reported with the green line. This part of the ribozyme is highly solvent exposed and is responsible in some case of the oscillatory behavior of the RMSD.

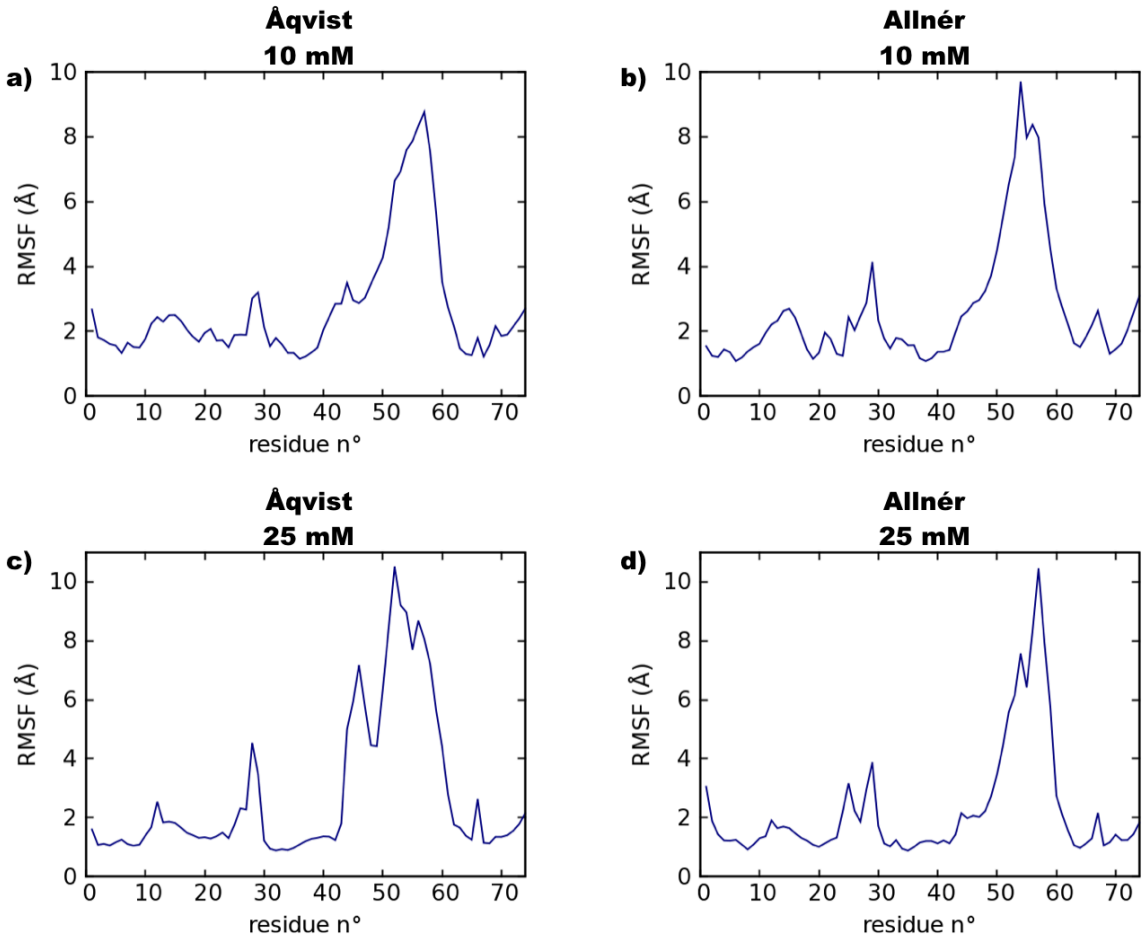

Figure S15. RMSF (Å) vs simulation time (ns) of the hepatitis delta virus (HDV) ribozyme with empirical Mg^{2+} force field parameters according to the Åqvist and Allnér models in (a) and (b), respectively, at [Mg^{2+}] =10 mM and to the Åqvist and Allnér in (c) and (d), respectively, at [Mg^{2+}] = 25 mM.

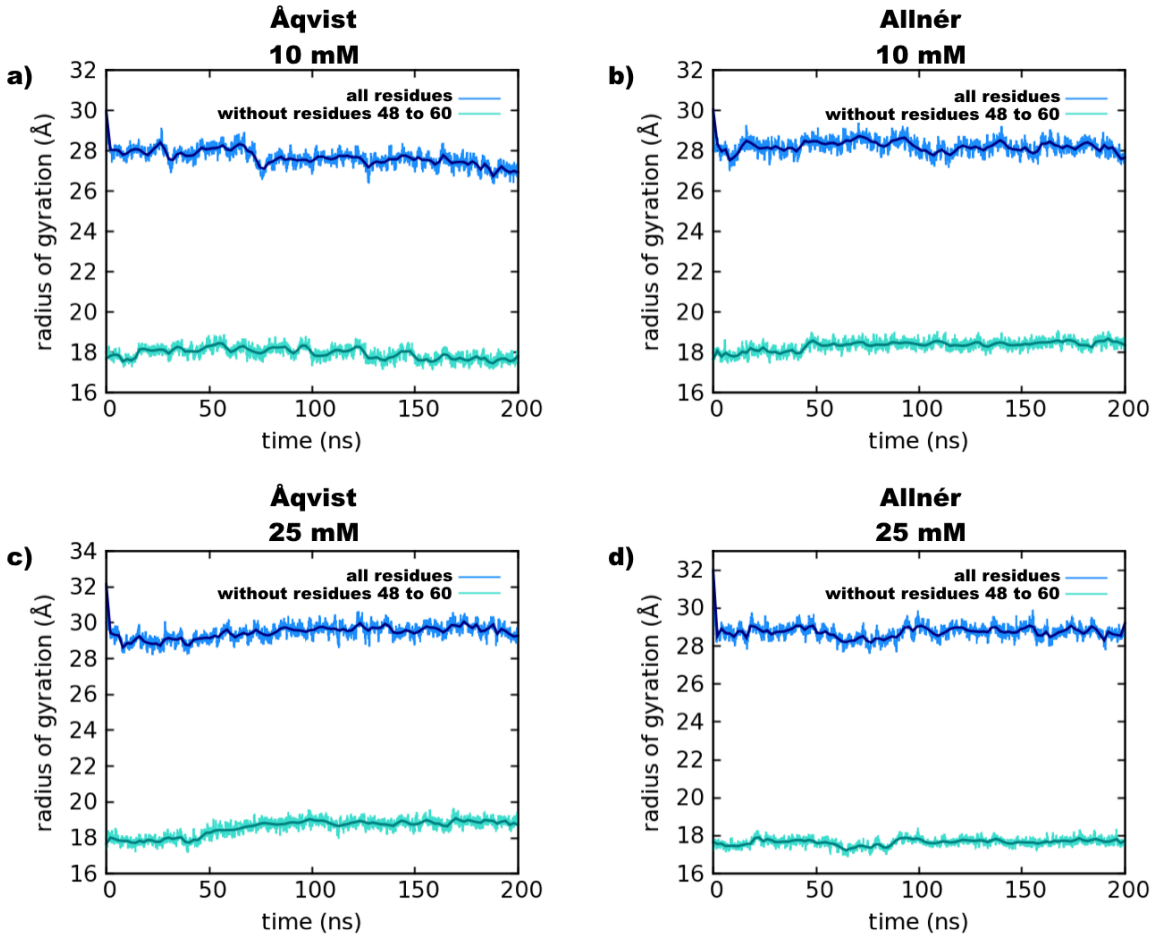

Figure S16. Radius of gyration (R_g) (Å) vs simulation time (ns) of the hepatitis delta virus (HDV) ribozyme with empirical Mg^{2+} force field parameters according to the Åqvist and Allnér models in (a) and (b), respectively, at [Mg^{2+}] =10 mM and to the Åqvist and Allnér in (c) and (d), respectively, at [Mg^{2+}] = 25 mM. The R_g without residues 48 to 60 is reported with the green line. This part of the ribozyme is highly solvent exposed and is responsible in some case of the oscillatory behavior of the R_g.

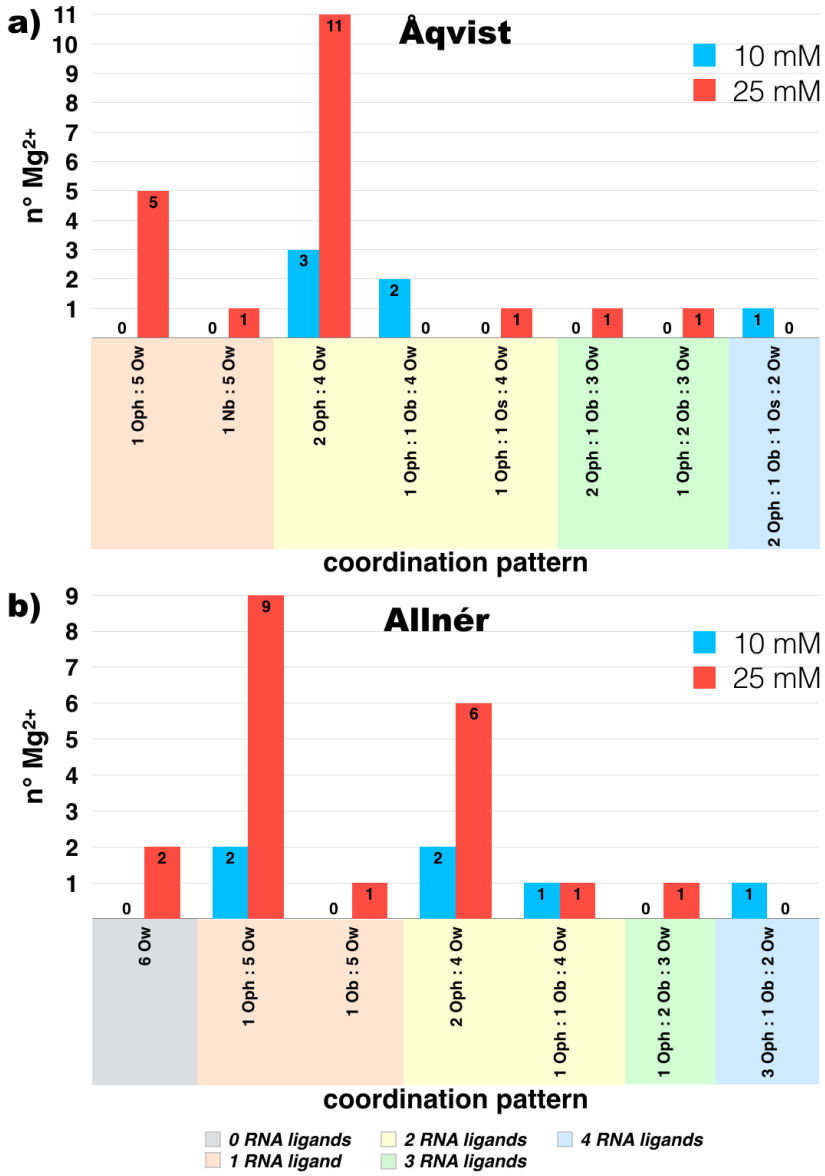

Figure S17. Histograms determining the population of the Mg^{2+}–RNA coordination patterns observed during MD simulations of the HDV ribozyme performed with the Åqvist (a) and Allnér (b) Mg^{2+} parameters at $[Mg^{2+}]$ = 10 mM (blue bars) and 25 mM (red bars). The *x-axis* reports the Mg^{2+} CPs identified from MD simulations. The number of RNA ligands (from 0 to 4) is highlighted with different colors. The *y-axis* reports the number of Mg^{2+} ions (i.e., population) having a specific CP. The most populated Mg^{2+}–RNA coordination patterns are $2O_{ph}$:$4O_w$ (Åqvist) and $1O_{ph}$:$5O_w$ (Allnér), with the Allnér parameters favoring more hydrated sites.

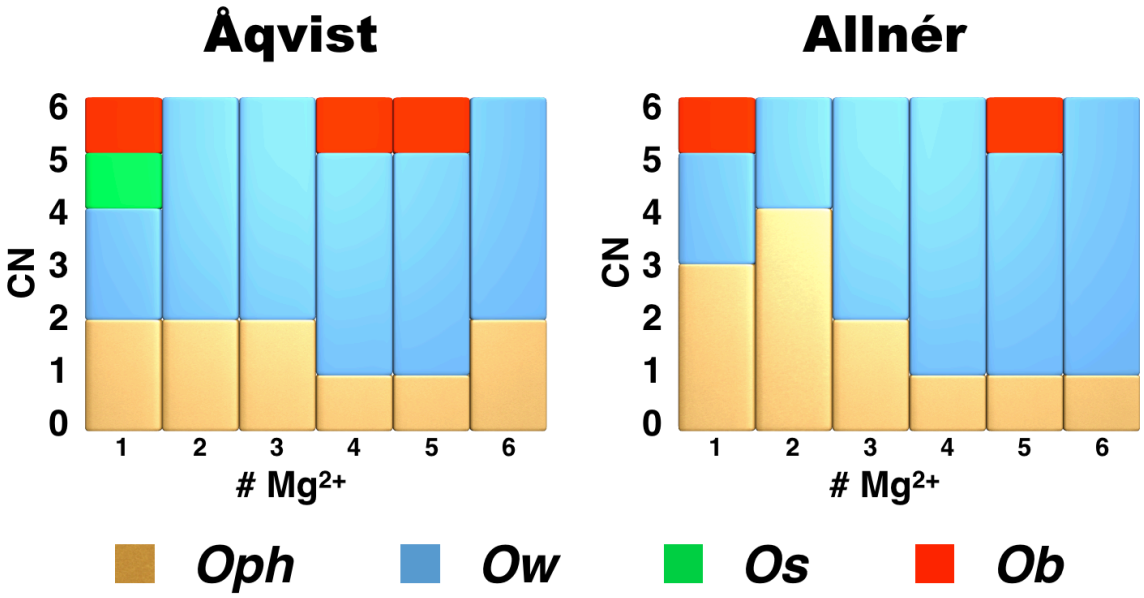

Figure S18. Histograms showing the composition of the coordination sphere of the Mg^{2+} *inner-sphere* sites in HDV as determined from MD performed with the Åqvist and Allnér parametrizations at [Mg^{2+}] = 10 mM. The *x-axis* reports the Mg^{2+} sites in HDV. The *y-axis* reports the *CN* for the Mg^{2+} coordination sphere. Donor atom types are identified with different colors as specified in the bottom legend.

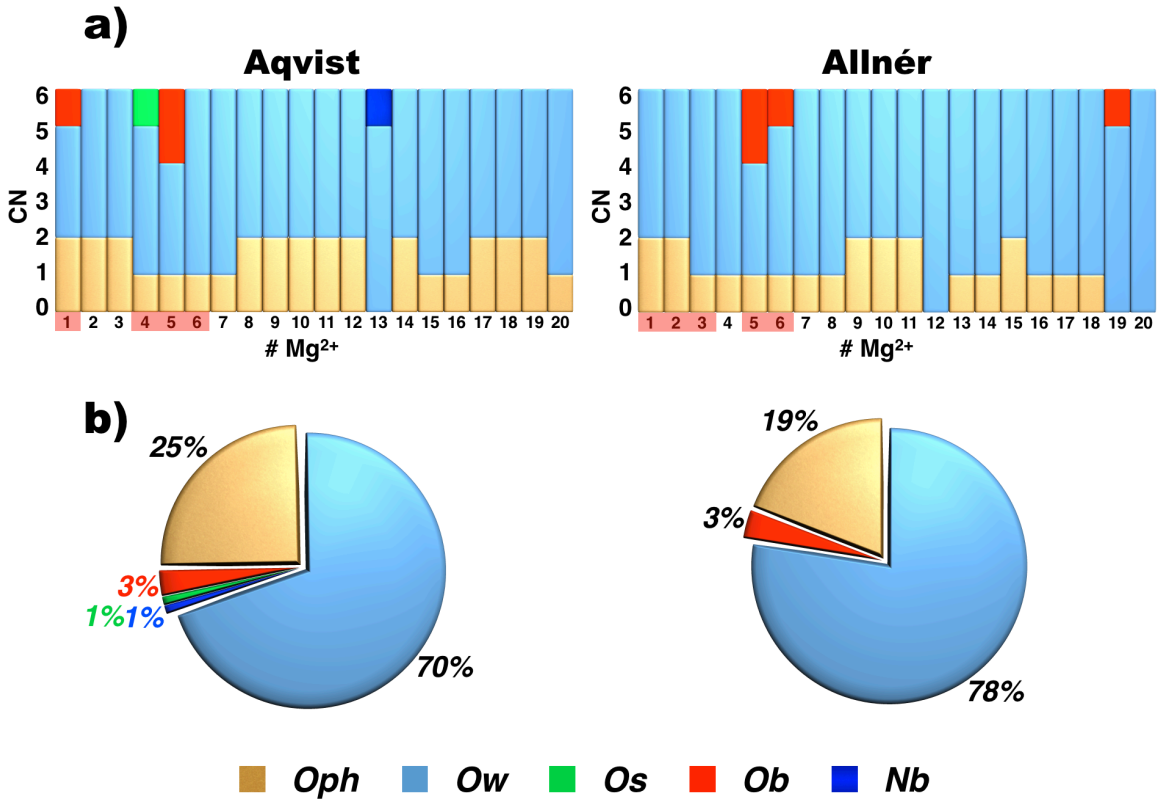

Figure S19. (a) Histograms showing the composition of the coordination sphere of the Mg^{2+} sites in HDV as determined from MD performed with the Åqvist and Allnér parametrizations at [Mg^{2+}] = 25 mM. The *x-axis* reports the Mg^{2+} sites in HDV. The *y-axis* reports the *CN* for the Mg^{2+} coordination sphere. The sites that change their ligand composition with respect to the simulation at [Mg^{2+}] = 10 mM are highlighted in red. Remarkably, for both Mg^{2+} models, only two of the six original sites preserve the same ligand composition at the two Mg^{2+} concentrations (see Figure S18). (b) Statistical distribution of different RNA ligands in the Mg^{2+} *inner-sphere* (expressed as percentages) as calculated from MD simulations of HDV performed with the Åqvist and Allnér parametrizations at [Mg^{2+}] = 25 mM. Donor atom types are identified with different colors as specified in the bottom legend.

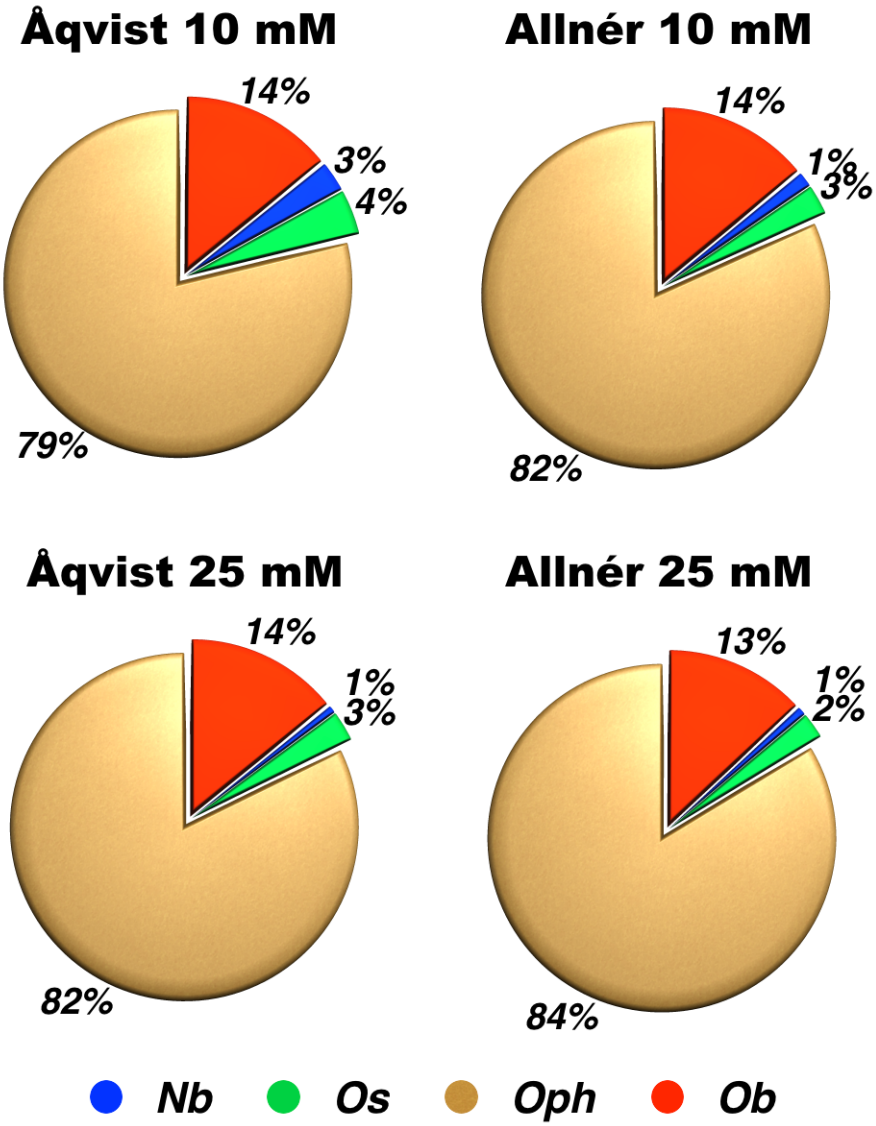

Figure S20. Statistical distribution of different RNA ligands in the Mg^{2+} *inner-sphere* (expressed as percentages) as calculated from MD simulations grouping the results of both the G*II*-I and the HDV according to the parametrization (Åqvist and Allnér) and the Mg^{2+} concentration conditions employed.

2.3 The Catalytic Site

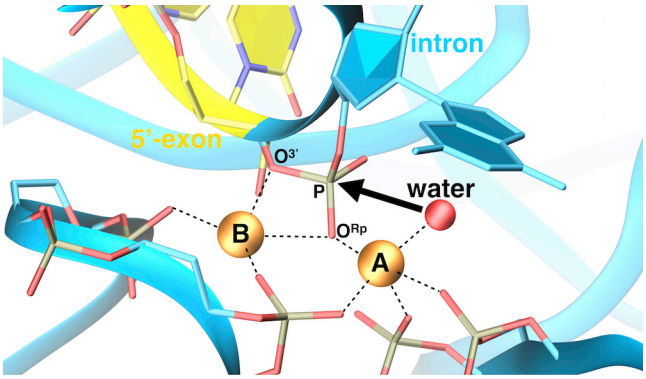

Figure S21. Active site from the crystal structure of the reactive adduct (PDB entry: 4FAQ).[10] The oxygen atom of the nucleophilic water molecule and the Mg^{2+} ions are shown as red and orange spheres, respectively. Phosphates are shown in licorice and are colored according to element. An arrow indicates the direction of the nucleophilic attack on the scissile phosphate.

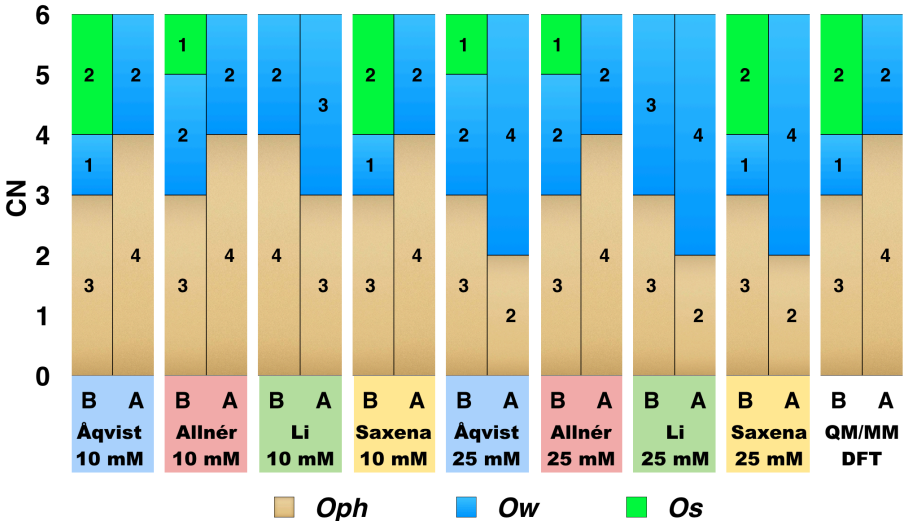

Figure S22. Histogram showing the composition of the two Mg^{2+} ions (A and B) of the catalytic site of G*II*-I ribozyme as reproduced the different Mg^{2+} force field models and by QM/MM MD simulations.[1-5] The QM/MM MD simulations were detailed in a previous study performed by us.[6]

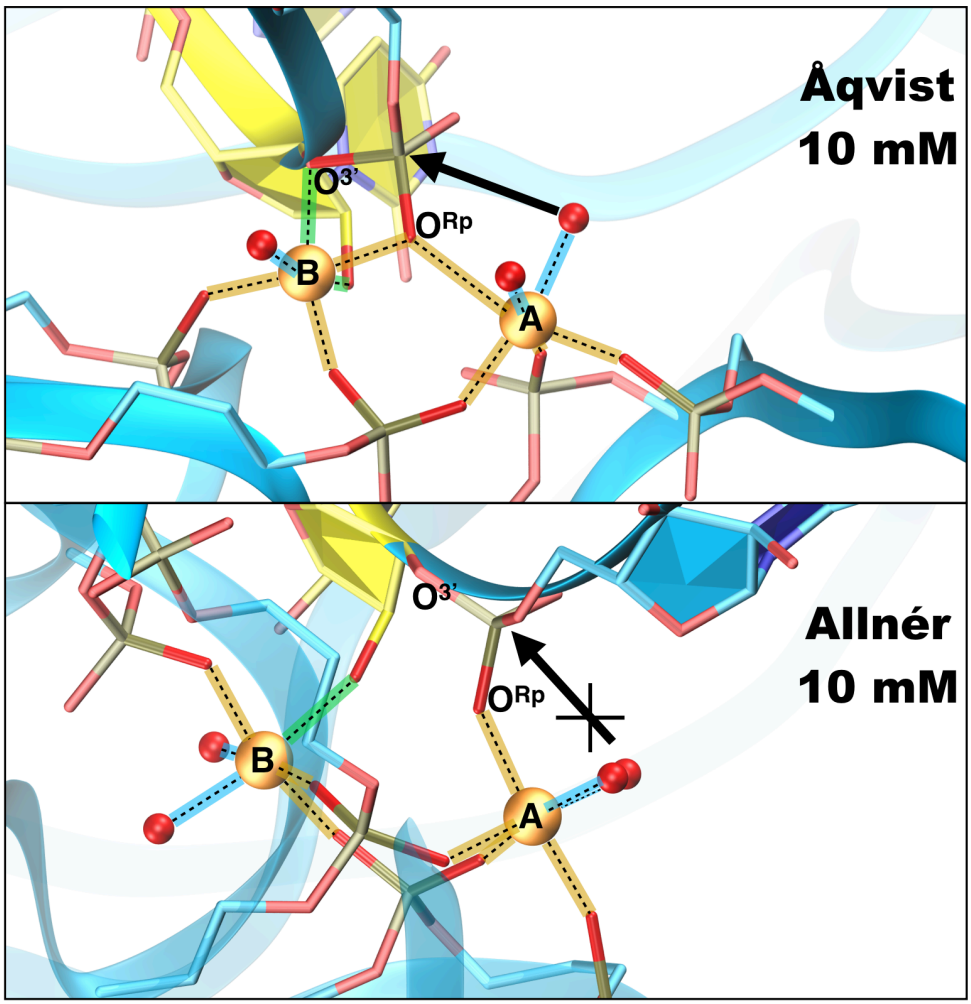

Figure S23. Snapshot of the catalytic site of G*II*-I ribozyme as obtained after 200 ns of classical MD simulations with the Åqvist and the Allnér model at [Mg^{2+}] = 10 mM. A complete distortion of Mg^{2+}-B coordination sphere is visible in the simulations performed with the Allnér model.

2.4 Density Functional Theory (DFT) Calculations

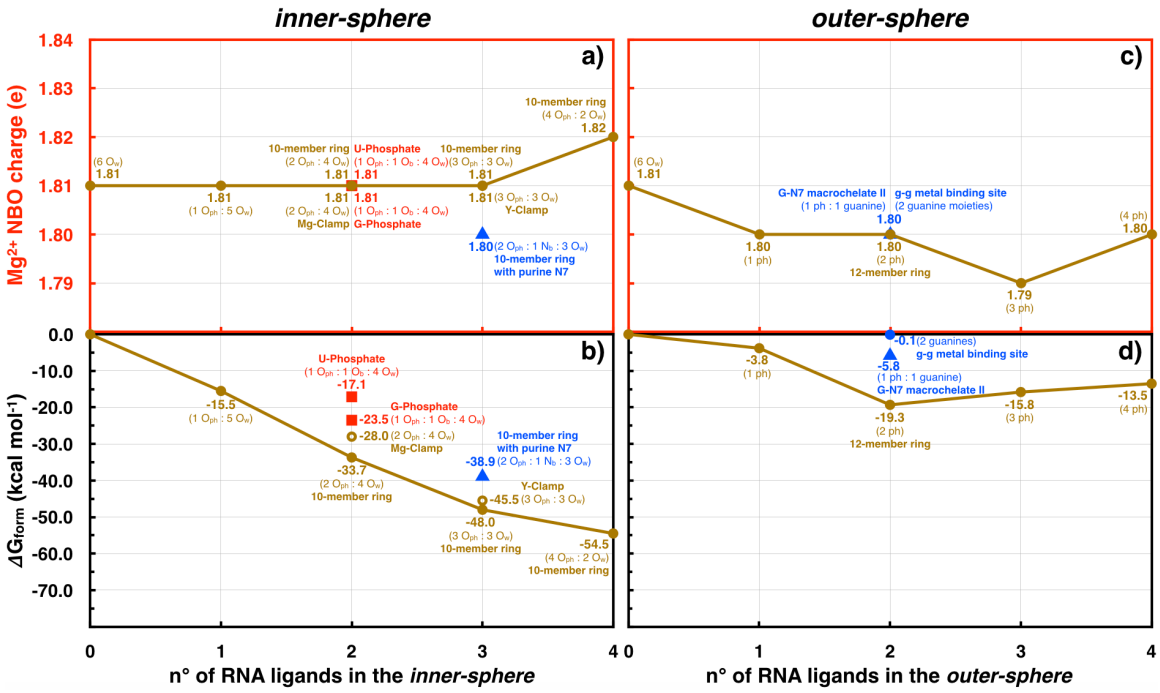

Figure S24. Mg^{2+} charge (e) and free energy of formation (ΔG_{form}, kcal/mol) of *inner-sphere* Mg^{2+} coordination sites, (a) and (b) respectively, and of *outer-sphere* Mg^{2+} coordination sites, (c) and (d) respectively, plotted as a function of the number of RNA ligands, and calculated at the DFT/B3LYP/6-311++G** level for the models shown in Figure 5a. The Natural Bond Orbital (NBO) charge is used to estimate the charge. Gold circles, red squares and blue triangles refer to model systems characterized by the presence of O_{ph}-only, at least one O_b or one N_b as non-water ligands, respectively. Model systems characterized by O_{ph} ligands only but corresponding to a different geometrical isomer are indicated with golden empty circles. For each model system the CP is reported in parenthesis.

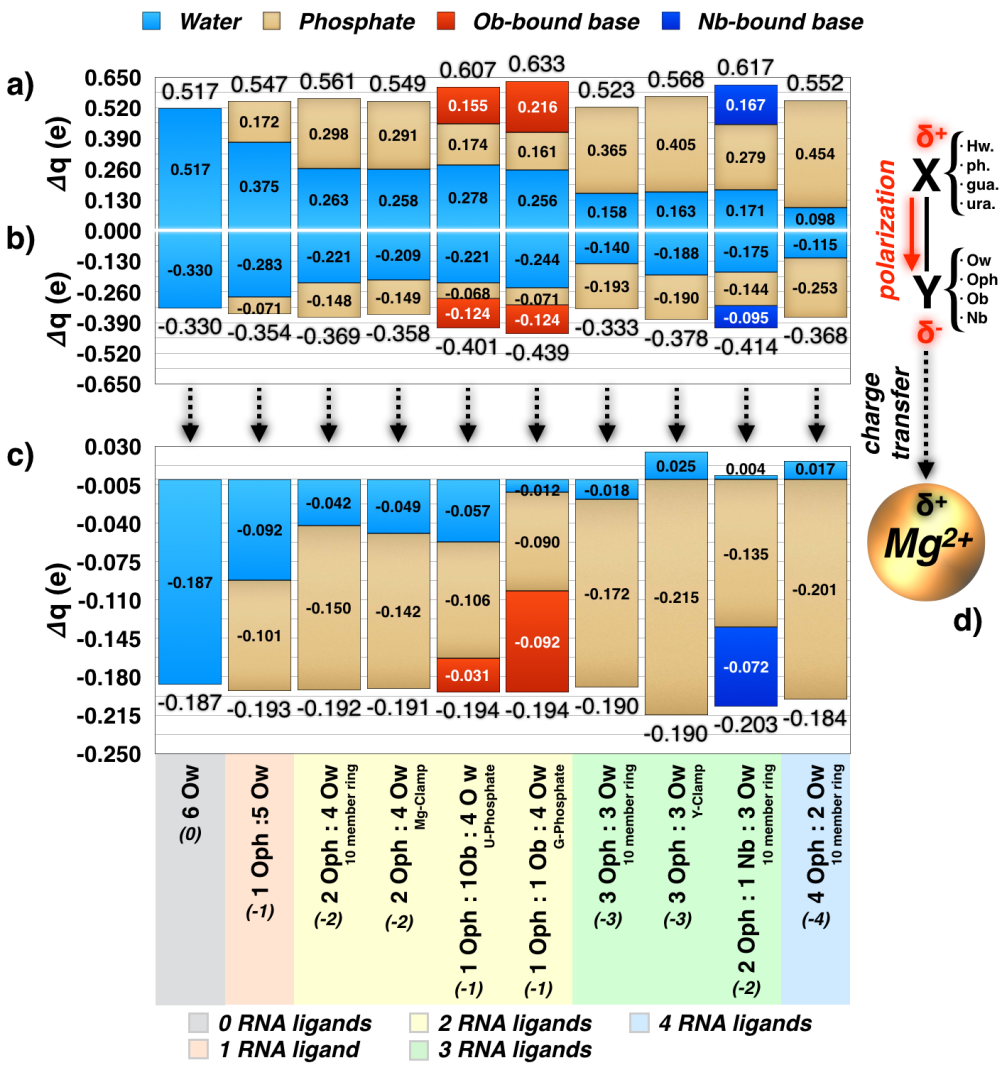

Figure S25. Charge rearrangements (Δq, e) of the (a) non-Mg^{2+}-coordinated and (b) Mg^{2+}-coordinated ligands atoms in the *inner-sphere* coordination sites; (c) amount of charge transferred (Δq, e) from the ligands towards Mg^{2+} ion calculated from the NBO charge distribution and the B3LYP functional with 6-311++G** basis set. Each contribution is dissected by atom type with light blue, gold, red and dark blue referring to water (O_w), phosphate (O_{ph}), nucleobases coordinated via O_b and N_b atoms, respectively. (d) Schematic picture of the polarization and charge transfer effects exerted by a Mg^{2+} ion. The formal charge of each CP is reported in parenthesis.

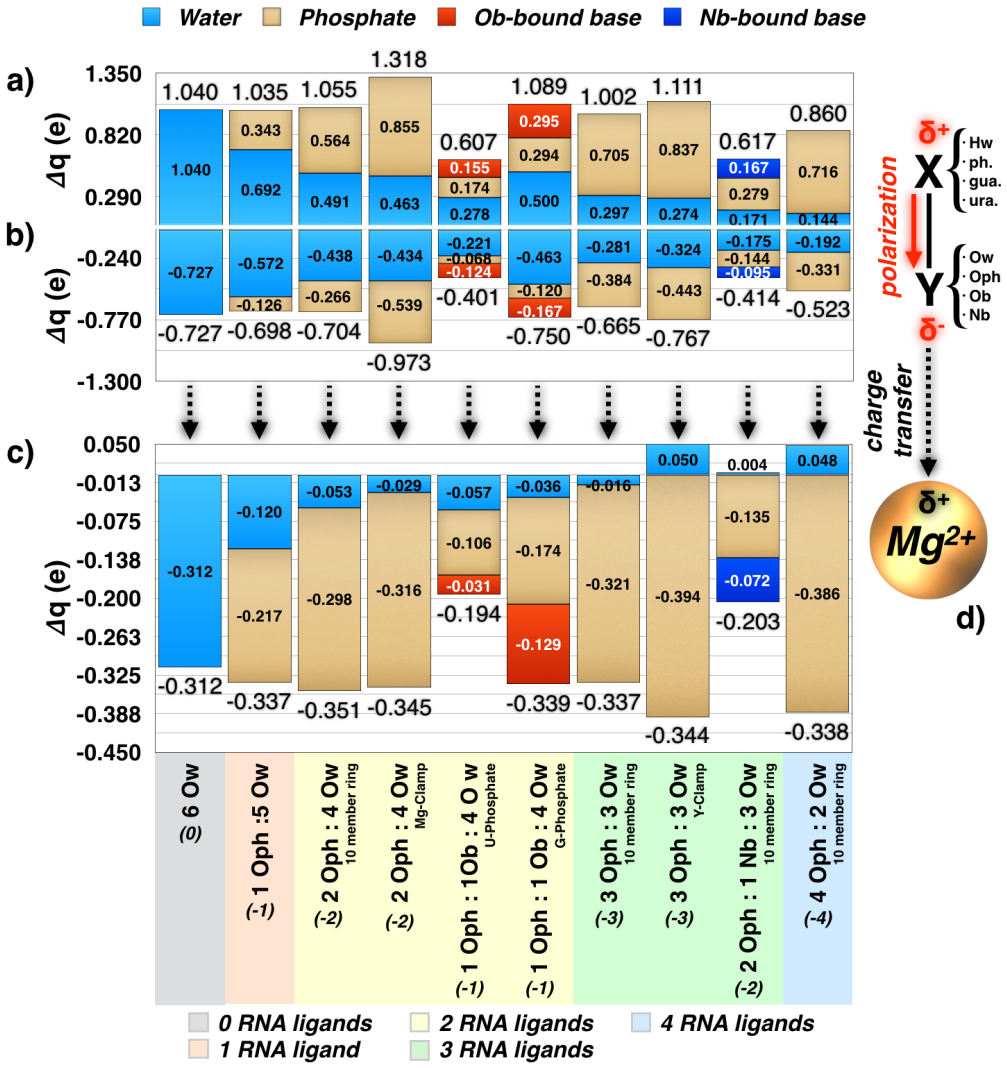

Figure S26. Charge rearrangements (Δq, e) of the (a) non-Mg^{2+}-coordinated and (b) Mg^{2+}-coordinated ligands atoms in the *inner-sphere* coordination sites; (c) amount of charge transferred (Δq, e) from the ligands towards Mg^{2+} ion calculated from the NBO charge distribution and the M06 functional with 3-21G basis set. Each contribution is dissected by atom type with light blue, gold, red and dark blue referring to water (O_w), phosphate (O_{ph}), nucleobases coordinated via O_b and N_b atoms, respectively. (d) Schematic picture of the polarization and charge transfer effects exerted by a Mg^{2+} ion. The formal charge of each CP is reported in parenthesis.

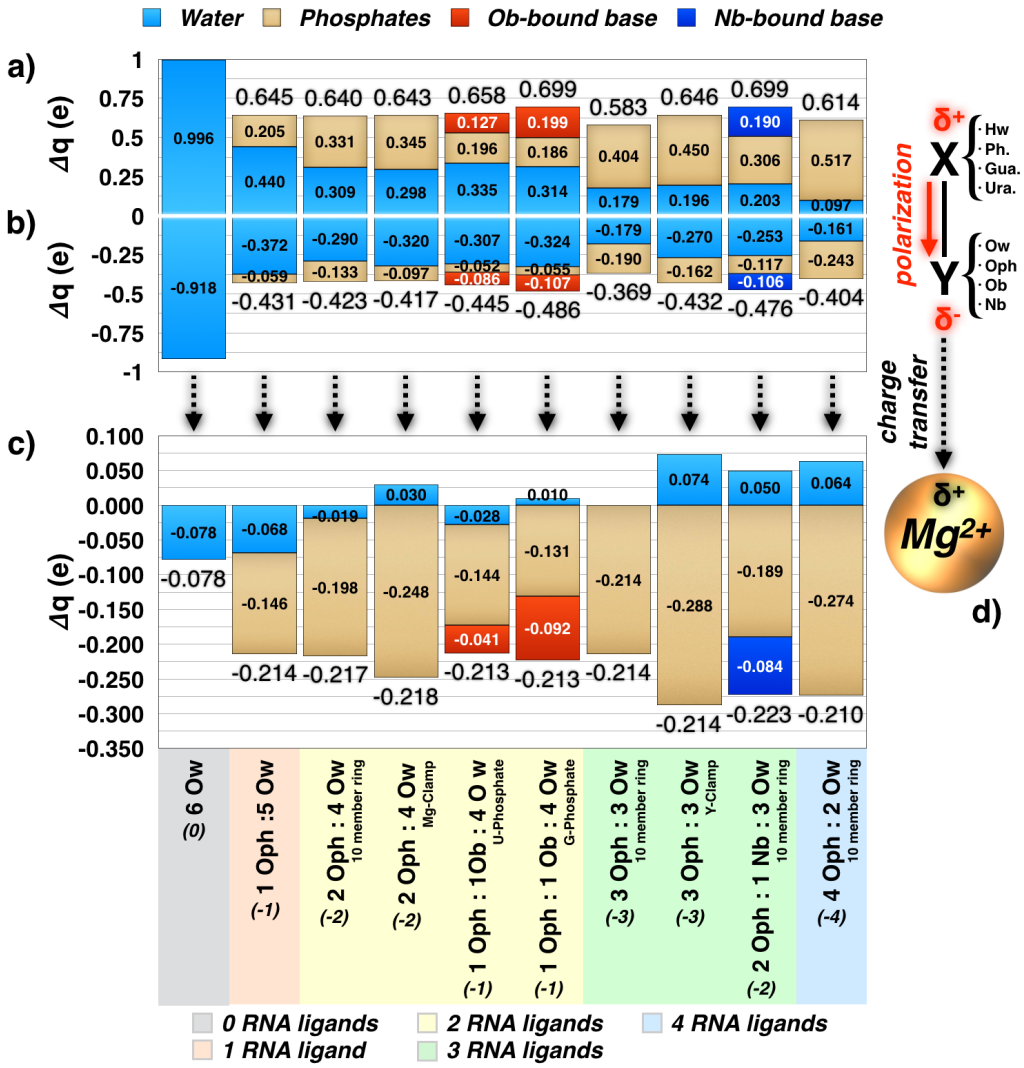

Figure S27. Charge rearrangements (Δq, e) of the (a) non-Mg^{2+}-coordinated and (b) Mg^{2+}-coordinated ligands atoms in the *inner-sphere* coordination sites; (c) amount of charge transferred (Δq, e) from the ligands towards Mg^{2+} ion calculated from the Bader charge distribution and the M06 functional with 6-311++G** basis set. Each contribution is dissected by atom type with light blue, gold, red and dark blue referring to water (O_w), phosphate (O_{ph}), nucleobases coordinated via O_b and N_b atoms, respectively. (d) Schematic picture of the polarization and charge transfer effects exerted by a Mg^{2+} ion. The formal charge of each CP is reported in parenthesis.

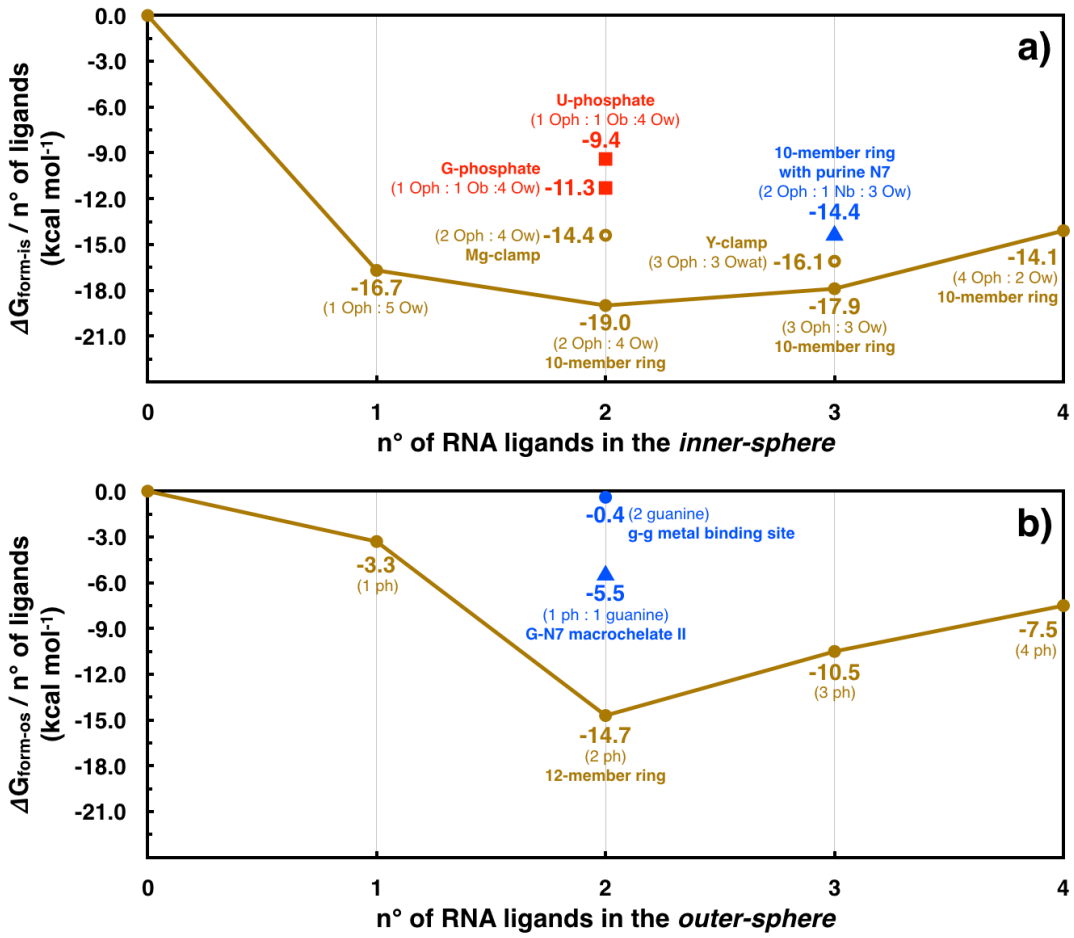

Figure S28. Average contribution to $\Delta G_{form\text{-}is}$ and $\Delta G_{form\text{-}os}$ per ligand in (a) and (b), respectively. Data come from simulations at the DFT/M06/6-311++G** level of theory.

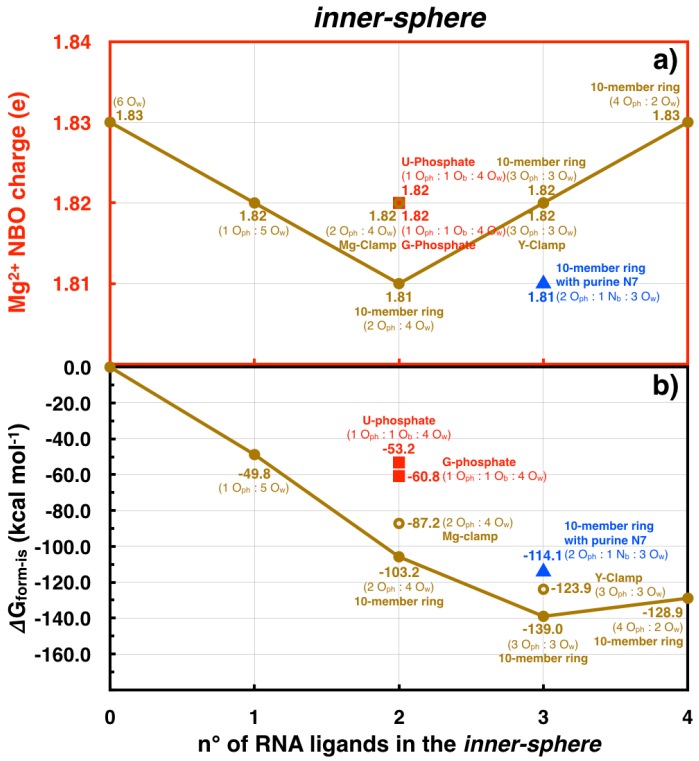

Figure S29. Mg^{2+} charge (e) and free energy of formation (ΔG_{form}, kcal/mol) of *inner-sphere* Mg^{2+} coordination sites, (a) and (b) respectively, plotted as a function of the number of RNA ligands, and calculated at the DFT/B3LYP/6-311++G** level for the models shown in Figure 5a. The Polarizable Continuum Model (PCM)[11] was used with a dielectric constant of 4. The Natural Bond Orbital (NBO) charge is used to estimate the charge. Gold circles, red squares and blue triangles refer to model systems characterized by the presence of O_{ph}-only, at least one O_b or one N_b as non-water ligands, respectively. Model systems characterized by O_{ph} ligands only but corresponding to a different geometrical isomer are indicated with golden empty circles. For each model system the CP is reported in parenthesis.

3. Supplementary Tables

Table S1. Force field (FF) vdW parameters (*A* and *B*, $Å^{12} \cdot$ kcal/mol and $Å^{6} \cdot$ kcal/mol) and charges (*q*, e) for fixed point charge (i.e., Åqvist, Allnér and Li) and CDA (i.e., Saxena and Oelschlaeger) models employed in this work.

NAME	$A_{Mg\text{-}Mg}$ ($Å^{12} \cdot$ kcal/mol)	$B_{Mg\text{-}Mg}$ ($Å^{6} \cdot$ kcal/mol)	$A_{d\text{-}d}$ ($Å^{12} \cdot$ kcal/mol)	$B_{d\text{-}d}$ ($Å^{6} \cdot$ kcal/mol)	q_{Mg} *(e)*	q_{d} *(e)*
Åqvist	225.26	28.39	-	-	+2	-
Allnér	2405.86	5.32	-	-	+2	-
Li	1673.12	8.26	-	-	+2	-
Saxena	729.00	278.89	0.0025	0.000	0	+0.333
Oelschlaeger	4901.75	1681.29	2.126	0.326	-1	+0.5

Table S2. Summary of the simulations length performed for the different systems investigated.

MODEL	G*II*-I Ribozyme		HDV Ribozyme	
	10 mM	**25 mM**	**10 mM**	**25 mM**
Åqvist	200 ns 100 ns 100 ns	100 ns	200 ns	200 ns
Allnér	200 ns 100 ns 100 ns	100 ns	200 ns	200 ns
Li	200 ns	100 ns	-	-
Saxena	200 ns	100 ns	-	-
Oelschlaeger	100 ns	-	-	-
SUBTOTAL	1300 ns	400 ns	400 ns	400 ns
TOTAL	2.5 μs			

Table S3. R_{max} (Å) of the radial distribution function (*g(r)*) for different Mg^{2+} ligand types, as reproduced by the Åqvist, Allnér, Li, Saxena and Oelshlaeger models. The Mg^{2+}–ligands coordination distance (Å), as calculated at the DFT/M06 level using the using the 6-311++g** basis set, is also reported (last row).

R_{max} (Å)					
Åqvist	**Oph**	**Ow**	**Os (O2' O3')**	**Ob (O6 O4)**	**N7**
	1.865	1.995	2.075	1.975	2.265
Allnér	**Oph**	**Ow**	**Os (O2')**	**Ob (O6 O4 O2)**	**N1 N7**
	1.965	2.055	2.135	2.045	2.295
Li	**Oph**	**Ow**	**Os**	**Ob (O6 O4 O2)**	**N7***
	1.935	2.035		2.015	-2.195
Saxena	**Oph**	**Ow**	**Os (O2' O3')**	**Ob (O6 O4)**	**N1 N7**
	2.035	2.165	2.175	2.085	
Oelschlaeger	**Oph**	**Ow**	**Os (O2' O3')**	**Ob (O6 O4 O2)**	**N1 N3 N7**
	2.235	2.365	2.325	2.285	2.465
DFT/M06	**Oph**	**Ow**	**Os (O2')**	**Ob (O6 O4 O2)**	**N1 N3 N7**
	2.03	2.115	2.12	2.07	2.225

4. References

(1) Aqvist, J. *J. Phys. Chem.* **1990**, *94*, 8021-8024.

(2) Allner, O.; Nilsson, L.; Villa, A. *J. Chem. Theory Comput.* **2012**, *8*, 1493-1502.

(3) Li, P. F.; Roberts, B. P.; Chakravorty, D. K.; Merz, K. M. *J. Chem. Theory Comput.* **2013**, *9*, 2733-2748.

(4) Oelschlaeger, P.; Klahn, M.; Beard, W. A.; Wilson, S. H.; Warshel, A. *J. Mol. Biol.* **2007**, *366*, 687-701.

(5) Saxena, A.; Sept, D. *J. Chem. Theory Comput.* **2013**, *9*, 3538-3542.

(6) Casalino, L.; Palermo, G.; Rothlisberger, U.; Magistrato, A. *J. Am. Chem. Soc.* **2016**, *138*, 10374-10377.

(7) Zheng, H. P.; Shabalin, I. G.; Handing, K. B.; Bujnicki, J. M.; Minor, W. *Nucleic Acids Res.* **2015**, *43*, 3789-3801.

(8) Boero, M.; Tateno, M.; Terakura, K.; Oshiyama, A. *J. Chem. Theory Comput.* **2005**, *1*, 925-934.

(9) Boero, M.; Park, J. M.; Hagiwara, Y.; Tateno, M. *J Phys Condens Matter* **2007**, *19*, 365217.

(10) Marcia, M.; Pyle, A. M. *Cell* **2012**, *151*, 497-507.

(11) Improta, R.; Barone, V.; Scalmani, G.; Frisch, M. J. *J. Chem. Phys.* **2006**, *125*, 054103.